Published in final edited form as:
Neuron. 2007 September 20; 55(6): 874–889. doi:10.1016/j.neuron.2007.06.041.

Postsynaptic Positioning of Endocytic Zones and AMPA Receptor Cycling by Physical Coupling of Dynamin-3 to Homer

Jiuyi Lu[2], **Thomas D. Helton**[2], **Thomas A. Blanpied**[2,#], **Bence Rácz**[3,†], **Thomas M. Newpher**[2], **Richard J. Weinberg**[3,4], and **Michael D. Ehlers**[1,2*]

1*Howard Hughes Medical Institute, Duke University Medical Center, Durham, NC 27710, USA*

2*Department of Neurobiology, Duke University Medical Center, Durham, NC 27710, USA*

3*Department of Cell and Developmental Biology, University of North Carolina School of Medicine, Chapel Hill, NC, 27599, USA*

4*Neuroscience Center, University of North Carolina School of Medicine, Chapel Hill, NC, 27599, USA*

Summary

Endocytosis of AMPA receptors and other postsynaptic cargo occurs at endocytic zones (EZs), stably positioned sites of clathrin assembly adjacent to the postsynaptic density (PSD). The tight localization of postsynaptic endocytosis is thought to control spine composition and regulate synaptic transmission and plasticity. However, the molecular mechanisms that situate the EZ near the PSD, and the role of local spine endocytosis in synaptic transmission, are unknown. Here we report that a physical link between dynamin-3 and the postsynaptic adaptor Homer positions the EZ near the PSD. Disruption of dynamin-3 or its interaction with Homer uncouples the PSD from the EZ, resulting in synapses devoid of postsynaptic clathrin. This loss of the EZ leads to a loss of synaptic AMPA receptors and reduced excitatory synaptic transmission that corresponds with impaired synaptic recycling. Thus, a physical link between the PSD and the EZ ensures localized endocytosis and recycling by recapturing and maintaining a proximate pool of cycling AMPA receptors.

Introduction

Rapid excitatory synaptic transmission at glutamatergic synapses is mediated by AMPA receptors, which are highly mobile at the postsynaptic membrane (Derkach et al., 2007). AMPA receptors, along with other postsynaptic membrane proteins, can diffuse out of the postsynaptic density (Tardin et al., 2003; Triller and Choquet, 2005; Ashby et al., 2006; Ehlers et al., 2007) and undergo dynamic intracellular trafficking through endocytosis and recycling (Luscher et al., 1999; Ehlers, 2000). Such endocytic trafficking is regulated by neuronal activity and mediates diverse forms of synaptic plasticity (Park et al., 2004; Brown et al., 2005; Park et al., 2006).

*Corresponding Author: Michael D. Ehlers, M.D., Ph.D., Howard Hughes Medical Institute, Department of Neurobiology, Duke University Medical Center, Box 3209, Durham, NC 27710, USA, Tel: (919)684-1828, FAX (919)668-0631, e-mail: ehlers@neuro.duke.edu.
#Present Address: Department of Physiology, University of Maryland School of Medicine, Baltimore, Maryland 21201,USA
†Present Address: Department of Anatomy and Histology, Faculty of Veterinary Science, Szent Istvan University, H-1078 Budapest, Istvan u. 2. Hungary.

Recent studies have found that the endocytosis of postsynaptic cargo occurs at endocytic zones (EZs), stably positioned sites of clathrin assembly adjacent to the postsynaptic density (PSD) (Blanpied et al., 2002; Racz et al., 2004). The tight localization of postsynaptic endocytosis is thought to control postsynaptic membrane composition and regulate diverse aspects of synaptic transmission and plasticity (Kennedy and Ehlers, 2006). However, the molecular mechanisms that position the endocytic machinery near the PSD, and the role of spine-localized endocytosis in synaptic transmission, are unknown.

In model mammalian cell lines, clathrin-mediated endocytosis occurs at discrete clathrin coat domains, uniformly distributed over the cell membrane with no known spatial relationship to other cellular structures (Gaidarov et al., 1999; Kaksonen et al., 2006). In contrast, clathrin puncta and coated pits on hippocampal neuron dendrites exhibit a highly specific localization a few hundred nanometers adjacent to the PSD (Blanpied et al., 2002; Racz et al., 2004). At the postsynaptic membrane, endocytic proteins such as clathrin and dynamin form part of the NMDAR/PSD-95 protein complex (Tu et al., 1998; Okamoto et al., 2001; Gray et al., 2003). In addition, both the PSD and the clathrin endocytic apparatus share common linkages to the actin cytoskeleton (Naisbitt et al., 1999; Gray et al., 2005; Kaksonen et al., 2006). Such studies suggest a molecular interface that directly or indirectly connects the PSD to endocytic structures.

Clathrin-mediated endocytosis is initiated by the recruitment of clathrin coat components to the plasma membrane, followed by invagination of the membrane to form a clathrin-coated pit (Kaksonen et al., 2006). Fission of clathrin-coated pits is mediated by large GTPases of the dynamin family, which oligomerize around the necks of invaginated pits (Praefcke and McMahon, 2004). Several studies have demonstrated an expanded role for dynamin as a scaffold that coordinates membrane dynamics and cytoskeletal reorganization at actin-rich regions of cells including membrane ruffles, podosomes, actin comets, mitotic cleavage furrows, and growth cones (Schafer, 2004; Kruchten and McNiven, 2006). Dynamins are targeted to these subcellular domains by protein interactions involving their C-terminal proline-rich domain (PRD) (Praefcke and McMahon, 2004). Such targeting may couple endocytosis to cytoskeletal remodeling at defined zones on the plasma membrane (Kruchten and McNiven, 2006).

To date, three different vertebrate dynamin genes have been identified (Cao et al., 1998). The brain-enriched dynamin-1 concentrates in the presynaptic terminal and plays a dominant role in synaptic vesicle endocytosis (Nakata et al., 1991). Dynamin-2 is expressed ubiquitously and similarly participates in membrane fission (Cook et al., 1994). In contrast, dynamin-3 is enriched in the brain and has been localized postsynaptically (Gray et al., 2003). Whereas dynamin-1 and -2 play important roles in membrane scission during endocytosis, the precise function of dynamin-3 is still undefined. Notably, dynamin-3 is the only dynamin isoform known to bind the postsynaptic adaptor Homer (Gray et al., 2003), potentially linking dynamin-3 to the PSD scaffold.

At the core of the dense postsynaptic protein network reside multivalent scaffolds of the Shank/ProSAP family (Naisbitt et al., 1999; Sheng and Hoogenraad, 2007). Shank interacts with numerous partners, including GKAP/SAPAP adaptor proteins which couple Shank to the NMDA receptor/PSD-95 complex (Naisbitt et al., 1999; Tu et al., 1999) and the small tetrameric adaptor Homer-1 (Tu et al., 1999; Hayashi et al., 2006), which couples Shank to diverse molecules including the IP3 receptor, metabotropic glutamate receptors (mGluRs), and dynamin-3 (Tu et al., 1998; Gray et al., 2003). Formation of a Shank-Homer complex promotes maturation of glutamatergic synapses, triggers the recruitment of synaptic AMPA receptors, and increases synaptic strength (Sala et al., 2001). Yet, little is known about the downstream effectors of Homer that regulate AMPA receptor abundance at the postsynaptic membrane.

In the present study, we have investigated the molecular mechanisms that link the EZ to the PSD and the function of spatially-localized endocytosis in excitatory synaptic transmission. Using a combination of live-cell imaging, electrophysiology, and quantitative light and electron microscopy, we demonstrate that dynamin-3 positions the clathrin endocytic machinery near the PSD through interaction with the postsynaptic scaffold complex Homer/Shank. Disruption of dynamin-3 uncouples the PSD from the EZ, leading to a loss of synaptic AMPA receptors and depresses excitatory synaptic transmission due to a failure of endocytosed receptors to locally recycle back to the synapse. These results define a direct physical link between the postsynaptic scaffold and spine trafficking machinery and demonstrate a novel requirement for localized endocytosis and recycling in maintaining a synaptically proximate pool of cycling AMPA receptors. Establishment of local endocytic cycling thereby links spatially delimited membrane trafficking to synapse-specific signaling.

Results

Clathrin Puncta are Firmly Positioned Just Lateral to the PSD

To examine the persistence and mobility of coated pits at PSD-associated endocytic zones (EZs), we monitored clathrin puncta in dendrites by confocal timelapse imaging. In the dendrites of cultured hippocampal neurons expressing PSD-95-GFP and clathrin-DsRed (18 days *in vitro*, DIV), clathrin-DsRed was distributed in a punctate pattern in the dendritic shaft and at sites adjacent to individual PSDs labeled by PSD-95-GFP (Figure 1A). To monitor the behavior of clathrin puncta, we used kymograph analysis to plot the fluorescence intensity of a line in the dendrite over time. Kymographs of clathrin spots near PSD-95 puncta consisted almost entirely of vertical bands stretching the duration of the timelapse, indicating that clusters of PSD-95-GFP and clathrin remain tightly associated with each other and are nearly immobile (Figure 1B and Supplementary Movie S1). In contrast, clathrin puncta at sites distant from the PSD were considerably more mobile (Figure 1B and Supplementary Movie S1). We occasionally observed mobile PSD-95 puncta moving along the dendrite at an average rate of 0.2 μm/min. Similar to previous observations (Gerrow et al., 2006), these mobile PSD-95 puncta contained Shank, Homer, and GKAP and likely represent a preformed complex. Surprisingly, mobile PSD-95 clusters continued to have an associated clathrin punctum (Figure 1C and Supplementary Movie S2). In addition, some PSDs underwent significant time-dependent changes in size and morphology, yet clathrin puncta always remained physically proximate (Figure 1D and Supplementary Movie S3). These data show that, unlike coated pits away from synapses, clathrin near the PSD is stable and remains in close proximity to the PSD.

Dynamin-3 Concentrates at Lateral Membrane Domains of Spines and Correlates with the Presence of an Endocytic Zone

Requisite for a molecule linking the PSD with the EZ is the ability to associate with components of the postsynaptic scaffold and with organizing proteins of the endocytic apparatus. We took advantage of the fact that 10–15% of dendritic spines in mature hippocampal neurons lack an EZ (Blanpied et al., 2002) to search for PSD scaffolds and endocytic proteins whose abundance in spines correlated with the presence of an EZ. From this, we identified dynamin-3, a member of the dynamin family of large GTPases. We selected dynamin-3 among candidate proteins for several reasons. First, dynamin-3 has been found to reside in postsynaptic compartments and a specific splice variant of dynamin-3 regulates dendritic spines (Gray et al., 2003; Gray et al., 2005). Second, dynamin-3 binds to the postsynaptic adaptor protein Homer1 (Gray et al., 2003). Third, dynamin-3 is homologous to, and may oligomerize with, dynamin-1 and dynamin-2, which are well studied components of the clathrin endocytic machinery (Praefcke and McMahon, 2004; Kruchten and McNiven, 2006). Fourth, dynamin-3 expression is largely restricted to brain and is upregulated during developmental periods of synapse formation (Gray et al., 2003; Gray et al., 2005).

Consistent with previous studies (Gray et al., 2003), immunostaining of cultured hippocampal neurons showed that dynamin-3 is highly enriched in dendritic spines (Figure 2A), and double labeling for dynamin-3 and PSD-95 revealed a partial overlap between these two proteins (data not shown) (Gray et al., 2003). To obtain a numerical index of spine targeting, we measured the ratio of fluorescence intensity between the spine head and the dendritic shaft, and found the spine/shaft ratio of endogenous dynamin-3 to be 2.8 fold higher than GFP (Figure 2B, n = 8 neurons, 270 spines, $p < 0.001$). To ensure that spine-localized dynamin-3 was postsynaptic and did not reflect presynaptic dynamin-3, we expressed dynamin-3-EGFP selectively in postsynaptic neurons. Under these conditions Dyn3-EGFP strongly localized to dendritic spines (Supplementary Figure S1A). Since 10–15% spines do not contain clathrin puncta (Blanpied et al., 2002), we wondered whether the presence of dynamin-3 correlated with the presence of EZ in spines. Hippocampal neurons expressing GFP and clathrin-DsRed were fixed and stained for dynamin-3 and the integrated fluorescent intensity was measured in spines separated into two groups according to the presence (EZ+) or absence (EZ−) of clathrin-DsRed. Visual inspection indicated that spines lacking dynamin-3 also lacked clathrin puncta (Figure 2C). Quantitative analysis revealed that spines containing endocytic zones (EZ+) had nearly 2.5-fold higher levels of dynamin-3 than EZ-negative spines (Figure 2D). Thus, the presence of dynamin-3 correlates with the presence of a spine EZ.

To determine the precise subcellular localization of dynamin-3 within spines, we performed immunogold electron microscopy on CA1 hippocampus stratum radiatum from adult rat. Consistent with previous studies (Gray et al., 2003), gold particles corresponding to dynamin-3 were localized to postsynaptic compartments of asymmetric synapses (Figure 3A). Presynaptic labeling was also observed (data not shown), but was not analyzed further. Within dendritic spines, dynamin-3 was sparse within the PSD, but was frequently observed at membrane domains lateral to the peripheral edge of the PSD (Figure 3A). To quantify the lateral position of dynamin-3, we measured the tangential distance of each particle away from the edge of the PSD along the plasma membrane (Racz et al., 2004) (see Experimental Procedures for details). Measurement of absolute distance showed that dynamin-3 was situated 324 ± 32 nm lateral to the PSD on average. To control for variation in spine size, particle positions were normalized such that 0 corresponded to the PSD edge and 1.0 to the point along the perimeter of the spine equidistant from both edges of the PSD. This analysis revealed that dynamin-3 concentrates at lateral spine membrane domains midway between the PSD edge and the furthest tangential point (normalized tangential position: 0.51 ± 0.03; Figure 3B). The observed lateral distribution of dynamin-3 was similar to that for clathrin (0.48 ± 0.02, 340 ± 15 nm) and the clathrin adaptor AP-2 (0.41 ± 0.02, 302 ± 24 nm) (Racz et al., 2004), defining the components of the spine EZ. Thus, dynamin-3 is properly situated to link the PSD and EZ.

Dynamin-3 Positions the EZ Near the PSD Through an Interaction with Homer-Shank

Members of the dynamin family interact with diverse proteins through their C-terminal proline-rich domains (PRDs), which are highly divergent among family members (Praefcke and McMahon, 2004) (Figure 4A). To test whether protein interactions involving dynamin-3 couple the EZ to the PSD, we first employed a dominant inhibitory strategy. Flag-tagged proline-rich domains (PRDs) of dynamins-1,-2, and -3 were expressed in hippocampal neurons to disrupt PRD-dependent interactions, together with PSD-95-GFP and clathrin-DsRed to mark the PSD and EZ, respectively. In control neurons, PSD-95-GFP puncta were nearly always associated with clathrin-DsRed (Figure 4B). In contrast, expression of the dynamin-3 proline-rich domain (Dyn3-PRD) resulted in a marked loss of PSD-associated clathrin puncta (Figure 4B). Expression of Dyn3-PRD did not change the total number of clathrin-positive puncta over dendrites (data not shown), supporting a selective defect in clathrin localization rather than clathrin coat formation.

For quantitative analysis, we measured the percentage of PSD-95-GFP puncta that lacked an EZ. Whereas normally very few PSDs lack an associated EZ (8.4 ± 1.8%, n = 134), expression of Dyn3-PRD caused a five-fold increase in the fraction of EZ-negative synapses (45.3 ± 3.7% EZ negative synapses, n = 20, $p < 0.001$ relative to control, t-test; Figure 4F). On the other hand, expression of Dyn1-PRD or Dyn2-PRD, both of which inhibit clathrin-mediated endocytosis (Luscher et al., 1999; Praefcke and McMahon, 2004), had minimal effect on the spatial positioning of clathrin puncta adjacent to the PSD (percent EZ-negative synapses: Dyn1-PRD, 13.3 ± 2.2%, n = 20; Dyn2-PRD, 13.0 ± 1.7%, n =16; $p > 0.05$ relative to control, t-test; Figure 4B and 4F). Thus, protein interactions involving the PRD of dynamin-3 couple the EZ to the PSD, while dynamin-dependent endocytosis *per se* is not required for localizing the spine endocytic machinery.

Conspicuous among proteins which uniquely bind the PRD of dynamin-3 is the postsynaptic adaptor Homer-1b/c (Gray et al., 2003), hereafter referred to as Homer. The Homer family of proteins mediates diverse protein-protein interactions through an N-terminal EVH1 domain that binds consensus PXXF motifs in target proteins (Tu et al., 1998). At the PSD, Homer interacts with members of the Shank/ProSAP family scaffold proteins (Shank 1–3, hereafter referred to as Shank) (Tu et al., 1999), and by virtue of its ability to oligomerize through a C-terminal coiled-coil tetramerization domain (Hayashi et al., 2006), Homer forms physical linkage between Shank and diverse protein targets including group I metabotropic glutamate receptors (mGluRs) and inositol-1,4,5-trisphophate (IP3) receptors (Tu et al., 1998; Tu et al., 1999). In addition, dynamin-3, but neither dynamin-1 nor dynamin-2, contains a PXXF motif within its PRD and is known to bind Homer (Gray et al., 2003). We hypothesized that, by binding both dynamin-3 and Shank, Homer could physically link the endocytic apparatus to the PSD scaffold (Figure 4C). Consistent with this notion, dynamin-3 was present in a biochemical complex with Homer1, Shank, and classic endocytic dynamins in brain (Figure 4D). Notably, expression of a point mutant of dynamin-3 unable to bind Homer, Dyn3-P800L, resulted in a marked loss of PSD-associated clathrin puncta (Figure 4E), and a corresponding increase in PSDs devoid of EZs (38.5 ± 2.3% EZ negative synapses, n = 34, $p < 0.001$ relative to control, t-test; Figure 4F). In contrast, expression of wildtype dynamin-3 had no effect on EZ positioning near the PSD (12.9 ± 3.9% EZ negative synapses, n = 15, $p > 0.05$ relative to control, t-test; Figure 4F). Moreover, whereas expression of Dyn3-PRD caused loss of the EZ (Figure 4B), introduction of the P800L mutation into Dyn3-PRD (Dyn3-PRDPL) abrogated its effect on EZ localization (11.2 ± 1.1% EZ negative synapses, n = 27, $p > 0.05$ relative to control, t-test; Figure 4F).

To exclude potential effects of exogenously expressed PSD-95-GFP, a parallel set of experiments was performed by transfecting GFP or GFP-tagged dynamin-3 constructs together with clathrin-DsRed in hippocampal neurons. Rather than PSD-95-GFP, staining for the vesicular glutamate transporter VGLUT1 was used to mark excitatory synapses, and the percentage of EZ-negative synapses was quantified as above. Quantitative analysis revealed no significant difference between these two sets of experiments (Supplementary Figure S2). Disruption of Homer binding by introduction of the P800L mutation did not change the spine enrichment of dynamin-3 (Supplementary Figure S1B), indicating that spine localization of dynamin-3 is not sufficient to conjoin the EZ and the PSD.

The above results support a requirement for EZ-PSD coupling by direct binding of dynamin-3 to Homer, perhaps via Shank (Figure 4C). To further test this model, we took advantage of Homer1a, a naturally occurring activity-induced isoform of Homer that lacks its C-terminal coiled-coil domain (Sala et al., 2003). Expression of Homer1a caused a marked increase in the fraction of synapses lacking a postsynaptic EZ (percent EZ-negative synapses: control, 8.4 ± 1.8%, n = 134; Homer1a, 38.7 ± 2.6%, n = 37; Figure 4G), that was quantitatively similar to that observed upon expression of Dyn3-PRD or Dyn3-P800L (Figure 4F). Next, we tested

whether the dynamin-3/Homer-dependent localization of the EZ required Homer binding to Shank. Indeed, expression of either a C-terminal fragment of Shank that binds Homer (Shank C-term) or a full-length Shank mutant lacking four amino acids required for Homer binding (ShankΔPLEF) (Sala et al., 2001; Sala et al., 2003) likewise resulted in a significant loss of PSD-associated clathrin puncta (percent EZ-negative synapses: Shank C-term, 43.7 ± 3.6%, n = 12; ShankΔPLEF, 36.8 ± 6.3%, n = 21; $p < 0.001$ relative to control, t-test; Figure 4G). Thus, a linear sequence of protein-protein interactions involving Shank, Homer, and dynamin-3 is required to localize EZ to the lateral margins of the PSD.

GTPase-Deficient Dynamin Mutants Do Not Affect EZ Localization

For dynamin-1 and dynamin-2, GTPase activity is required for vesicle fission during endocytosis (Praefcke and McMahon, 2004; Kruchten and McNiven, 2006). To examine whether the GTPase activity of dynamin-3 is likewise involved in endocytosis, we performed transferrin (Tf) uptake assay in COS7 cells. As expected, expression of Dyn1-K44A and Dyn2-K44A, which lack GTPase activity, inhibited Tf endocytosis (Supplementary Figure S3). Similarly, expression of Dyn3-K44A markedly reduced Tf uptake in COS7 cells (Supplementary Figure S3). In contrast, Tf uptake was unaffected by expression of Dyn3-P800L (Supplementary Figure S3). Thus, the highly conserved GTPase activity of dynamin-3, but not Homer binding, participates in endocytosis.

We next tested whether the GTPase activity of dynamin-3 is required for localizing the endocytic machinery to the PSD. Unlike mutation of its Homer-binding domain (Figure 4F), disruption of the GTPase activity of dynamin-3 had no effect on the synaptic localization of the EZ (Figure 4H). In fact, GTPase-deficient mutants of all dynamin isoforms failed to affect the localization of clathrin puncta adjacent to the PSD (percent EZ-negative synapses: GFP, 15.3 ± 2.7%, n = 20; Dyn1-K44A, 11.8 ± 1.1%, n = 15; Dyn2-K44A, 16.0 ± 1.6%, n = 12; Dyn3-K44A, 20.4 ± 6.1%, n = 16; $p > 0.05$; Figure 4H). These data show that dynamin-dependent endocytosis is not required to position clathrin near the postsynaptic membrane.

Neither Actin Remodeling Nor Lipid Binding Mediate EZ Localization

To assess potential effects of expressed dynamin mutants on spine actin, F-actin content in spines was measured by phalloidin staining. Quantitative analysis revealed no difference in spine F-actin content between neurons expressing Dyn3-PRD or Dyn3-P800L and GFP control cells (Supplementary Figures S4A and S4B). The turnover rate of actin was further analyzed by fluorescence recovery after photobleaching (FRAP) and no change was observed in neurons expressing Flag-Dyn3-P800L compared with cells transfected with empty vector or Flag-Dyn3 wildtype (Supplementary Figure S4C). These data indicate that actin dynamics are not significantly affected upon expressing dynamin-3 mutants, demonstrating that disruption of the EZ is not a secondary effect of actin perturbation.

To further analyze the domains of dynamin-3 required to link the EZ and PSD, we generated dynamin mutants unable to bind cortactin (Dyn3-Δ819–831; Supplementary Figure S5) or incapable of binding phosphoinositides at the plasma membrane (Dyn3-ΔPH; Supplementary Figure S6) (Praefcke and McMahon, 2004; Schafer, 2004; Gray et al., 2005). Intriguingly, neither of these dynamin-3 mutants caused loss of postsynaptic EZ at glutamatergic synapses (Supplementary Figure S5B, S5C, and Figure S6D). Moreover, neither Dyn3-Δ819–831 nor Dyn3-ΔPH affected spine enrichment (Supplementary Figure S1B). In contrast, expression of Dyn3-ΔPH significantly reduced Tf uptake in COS7 cells (Supplementary Figure S6B and S6C). Thus, whereas Homer binding to dynamin-3 is required to couple the EZ to the PSD, cortactin binding and phosphoinositide binding are not.

Coupling the EZ to the PSD Requires Oligomerization of Postsynaptic Dynamins

How then does dynamin-3 bound to Homer bridge the endocytic machinery? Previous studies have shown that dynamin-1 and dynamin-2 can homo- or hetero-oligomerize to form large stacked ring structures via their GTPase effector domain (GED) (Okamoto et al., 1999; Praefcke and McMahon, 2004). To examine whether dynamin-3 can form oligomers, co-immunoprecipitations were performed from lysates of HEK 293T cells transfected with Flag- and GFP-tagged dynamins. Both GFP-Dyn3 and GFP-Dyn2 co-immunoprecipitated with Flag-Dyn3 (Figure 5B), indicating that dynamin-3 can form homo-oligomers with itself and hetero-oligomers with dynamin-2. Disrupting the Homer-binding domain of dynamin-3 (Dyn3-P800L) had no effect on its ability to oligomerize (Figure 5B).

We next tested whether oligomerization of dynamin-3 is required for localizing the EZ near the PSD. For this, we expressed a dynamin-3 mutant lacking the GTPase effector domain (GED) which is required for oligomerization (Okamoto et al., 1999) (Figure 5A). Interestingly, oligomerization-deficient dynamin-3 failed to enrich in dendritic spines (Supplementary Figure S1B) and expression of Dyn3-ΔGED caused a dramatic increase in the fraction of EZ-negative synapses (percent EZ-negative synapses: GFP, 13.3 ± 2.3 %, n = 14; Dyn3-ΔGED, 43.7 ± 2.4 %, n = 11; $p < 0.001$ relative to control; Figure 5C and 5D). Thus, oligomerization of dynamin-3, either with itself or with dynamin-2, is required for positioning the EZ adjacent to the PSD. These findings support a bifunctional model whereby dynamin-3 couples to the PSD via its PRD and to the endocytic machinery by its ability to oligomerize with other dynamins.

Loss of Endogenous Dynamin-3 Uncouples the Endocytic Machinery from the PSD

To examine the role of endogenous dynamin-3 in positioning spine EZ, we next employed an RNA interference (RNAi) strategy for loss-of-function analysis. We tested several siRNA duplexes targeting dynamin-3 (*d3RNAi*) in HEK 293T cells (Supplementary Figure S7A) and from these designed two short hairpin RNA (shRNA) plasmids targeting sequences specific for dynamin-3 (*d3RNAi-2*, *d3RNAi-4*). The plasmids also expressed GFP from a separate promoter allowing identification of RNAi-expressing cells. Both *d3RNAi-2* and *d3RNAi-4* were selective for dynamin-3 and did not affect the expression of β-tubulin or dynamin-2 (Supplementary Figure S7A and S7B). In hippocampal neurons, expression of either *d3RNAi-2* or *d3RNAi-4* caused a significant decrease in endogenous dynamin-3 relative to a scrambled RNAi control (Supplementary Figure S7C and S7D). Knock-down of dynamin-3 had a small effect on spine size in young neurons (DIV 6–14), but was not studied further (Supplementary Figure S8).

To examine the effect of dynamin-3 knock-down on the localization of EZ, hippocampal neurons were transfected with RNAi constructs along with clathrin-DsRed. Excitatory synapses were visualized by VGLUT1 staining. EZ-positive or negative synapses were defined as above. Expression of either *d3RNAi-2* or *d3RNAi-4* resulted in a marked loss of synapse-associated clathrin puncta (percent EZ-negative synapses: scramble, 23.7 ± 2.5%, n = 36; *d3RNAi-2*, 58.4 ± 2.9%, n = 41; *d3RNAi-4*, 48.2 ± 3.3%, n = 40; $p < 0.001$; Figure 6). In contrast, knock-down of dynamin-2 had no effect on EZ positioning in spines (*d2RNAi-2*, 22.0 ± 2.0% EZ-negative synapses, n = 13, $p > 0.05$; Figure 6C). The effect of dynamin-3 RNAi knock-down was completely rescued by co-expression of dynamin-3 cDNAs containing silent mutations (Dyn3-2* and Dyn3–4*) that rendered the dynamin-3 mRNA resistant to the specific sequences targeted by *d3RNAi-2* and *d3RNAi-4* respectively (percent EZ-negative synapses: scramble, 23.7 ± 2.5%, n = 36; *d3RNAi-2* + Dyn3-2*, 24.9 ± 1.2%, n = 18; *d3RNAi-4* + Dyn3-4*, 25.4 ± 2.0%, n = 25; $p > 0.05$; Figure 6C and Supplementary Figure S7E). In addition, neither RNAi-resistant dynamin-3 unable to bind Homer (Dyn3-4*-P800L) nor Dyn3-ΔGED which lacks the *d3RNAi-2* recognition sequence was able to rescue the loss of PSD-associated

clathrin induced by dynamin-3 RNAi (percent EZ-negative synapses: *d3RNAi-4* + Dyn3-4*-P800L, 42.2 ± 4.2 %, n =10; *d3RNAi-2* + Dyn3-ΔGED, 47.9 ± 2.7 %, n = 16; $p < 0.001$; Figure 6C). Thus, loss of endogenous dynamin-3 uncouples the endocytic machinery from the PSD, and this effect can be rescued by wildtype dynamin-3, but not by mutant dynamin-3 lacking domains required for oligomerization or Homer binding.

The EZ Maintains Synaptic AMPA Receptors

Given the above findings that Homer binding to dynamin-3 localizes the endocytic machinery near the PSD (Figure 4 and Figure 6), together with the known regulation of AMPA receptors by endocytic cycling (Luscher et al., 1999;Ehlers, 2000;Park et al., 2004), we hypothesized that local positioning of the EZ could participate in AMPA receptor synaptic trafficking. Considering that 10–15% of glutamatergic synapses lack an EZ, we first asked whether these synapses had more or fewer AMPA receptors. Surface labeling of GluR1 AMPA receptors revealed that synapses lacking a clathrin EZ had fewer AMPA receptors (Figure 7A). Quantitative analysis revealed a nearly 50% reduction in surface GluR1 at synapses lacking a PSD-associated EZ (Figure 7B). Thus, perhaps paradoxically, the presence of an EZ correlates positively with the abundance of synaptic AMPA receptors.

We next tested whether forced loss of the EZ by disruption of dynamin-3 altered synaptic AMPA receptors. Indeed, expression of either Dyn3-PRD or Dyn3-P800L, which uncouple the EZ from the PSD (Figure 4), led to a significant loss of surface GluR1 from glutamatergic synapses (normalized synaptic surface GluR1: GFP, 100 ± 0.9%, n = 20; Dyn3-PRD, 65.8 ± 0.6%, n = 31; Dyn3-P800L, 69.1 ± 0.6%, n = 21; $p < 0.001$; Figure 7C and 7D). Similar results were obtained for synaptic GluR2 receptors (Supplementary Figure S9). Moreover, uncoupling of the EZ from the PSD produced a marked decrease in the AMPAR/NMDAR ratio at glutamatergic synapses (GFP, 1.00 ± 0.08, n =15; Dyn3-PRD, 0.64 ± 0.07, n = 16; Dyn3-P800L, 0.62 ± 0.08, n = 11; $p < 0.001$; Figures 7E and 7F), and an increase in NMDAR-only morphologically ‘silent’ synapses (GFP, 32.4 ± 3.3%; Dyn3-P800L, 73.2 ± 4.8%; Dyn3-PRD, 56.6 ± 6.5%; $p < 0.001$; Figure 7G), suggesting a potential role for the spine EZ in the initial acquisition of AMPA receptors during glutamatergic synapse maturation. Importantly, disruption of the EZ by knock-down of endogenous dynamin-3 (Figure 6 and Supplementary Figure S7) likewise resulted in a significant loss of surface GluR1 at synapses (normalized surface synaptic GluR1: scramble, 100 ± 0.6%, n = 58; *d3RNAi-2*, 63.7 ± 0.9%, n = 36; *d3RNAi-4*, 62.2 ± 0.8%, n = 38; $p < 0.001$; Figure 7H), and this effect could be rescued fully or in part by co-expression of RNAi-resistant dynamin-3 (surface synaptic GluR1 relative to GFP control: *d3RNAi-2*+ Dyn3-2*, 83.5 ± 1.1%, n = 24; *d3RNAi-4* + Dyn3–4*, 99.0 ± 1.5%, n = 16; $p < 0.001$ compared with corresponding *d3RNAi*; Figure 7H). RNAi-resistant dynamin-3 unable to bind Homer (Dyn3-4*-P800L) failed to rescue the loss of synaptic AMPA receptors induced by dynamin-3 RNAi (*d3RNAi-4* + Dyn3-4*-P800L, 66.6 ± 0.7 %, n = 19; $p < 0.001$; Figure 7H). These findings demonstrate that spatial proximity of the endocytic machinery maintains AMPA receptors at the postsynaptic membrane. Conversely, loss of the EZ results in the loss of synaptic AMPA receptors.

The Endocytic Zone Sustains Excitatory Synaptic Transmission

To determine the functional consequences of uncoupling the EZ from the PSD, dynamin-3 mutants or dynamin-3 shRNAs were expressed in hippocampal neurons and miniature excitatory postsynaptic currents (mEPSCs) were recorded using whole-cell voltage clamp. In control GFP transfected neurons, average mEPSC amplitudes and frequencies (23.1 ± 0.6 pA, 2.3 ± 0.1 Hz, n = 20) were significantly larger than in neurons expressing Dyn3-PRD (16.5 ± 0.8 pA, 1.4 ± 0.1 Hz, n = 18, $p < 0.001$ unpaired t-test) or Dyn3-P800L (14.7 ± 0.5 pA, 1.6 ± 0.1 Hz, n = 20, $p < 0.001$ unpaired t-test; Figure 8A–C). Thus, disruption of the dynamin-3/Homer interaction reduces synaptic strength.

Similarly, whereas expression of a scrambled shRNA had no effect on mEPSCs (21.4 ± 0.8 pA, 2.1 ± 0.1 Hz, n = 19, p > 0.05 relative to GFP, unpaired t-test), expression of shRNAs directed against dynamin-3 significantly decreased mEPSC amplitudes and frequencies (*d3RNAi-2*, 16.0 ± 0.5 pA, 1.6 ± 0.1 Hz, n = 13; *d3RNAi-4*, 16.3 ± 0.8 pA, 1.6 ± 0.1 Hz, n = 16; p < 0.001 unpaired t-test; Figure 8A–C), indicating that endogenous dynamin-3 supports basal excitatory transmission. Specificity of the dynamin-3 knock-down effect was confirmed by co-expression of RNAi-resistant dynamin-3, which restored synaptic transmission (*d3RNAi-2* + Dyn3-2*, 23.0 ± 0.6 pA, 2.4 ± 0.1 Hz, n = 15; *d3RNAi-4* + Dyn3-4*, 24.6 ± 0.5 pA, 2.3 ± 0.1 Hz, n = 13; p > 0.05 relative to scrambled shRNA control, unpaired t-test; Figures 8B and 8C). Taken together, these results demonstrate that the tight coupling of the EZ with the postsynaptic specialization maintains AMPA receptors at the synapse, effectively sustaining excitatory synaptic transmission.

Perisynaptic Positioning of the EZ Ensures Local Cycling and Recapture of AMPA Receptors

How does the spine EZ promote synaptic accumulation of AMPA receptors? In other cellular contexts, endocytosis of surface membrane proteins is followed by rapid and often local re-delivery back to the plasma membrane (Washbourne et al., 2004; Marco et al., 2007). We hypothesized that the spatial arrangement of the EZ immediately lateral to the PSD might serve to capture AMPA receptors released from the PSD for rapid local recycling to the spine plasma membrane allowing reincorporation back into the PSD scaffold (EZ+, Figure 9A). If so, the absence of an adjacent EZ would permit AMPA receptors released from the PSD to diffuse away from the synapse, leading to progressive loss of receptors over time (EZ−, Figure 9A). Since synaptic AMPA receptors would need to diffuse greater distances from the PSD to be endocytosed, this model predicts that uncoupling the EZ from the PSD should slow the initial uptake kinetics of AMPA receptors without affecting the absolute amount of AMPA receptor internalization. To test this possibility, we followed the endocytosis of endogenous GluR1 in hippocampal neurons using live cell antibody feeding assays (Figure 9B, see Supplemental Methods for details). In GFP-expressing control neurons, GluR1 endocytosis was rapid (Figures 9B and 9C). In contrast, expression of either Dyn3-PRD or Dyn3-P800L to disrupt the EZ led to a significant slowing of AMPA receptor endocytosis over the first 20 min (percentage of internalized GluR1 at 5 min: GFP 21.1 ± 1.8 %, n = 17; Dyn3-PRD, 9.8 ± 1.7 %, n = 20; Dyn3-P800L, 7.8 ± 1.8 %, n = 20; percent at 20 min: GFP, 30.1 ± 1.5 %, n = 20; Dyn3-PRD, 23.9 ± 2.0 %, n = 20; Dyn3-P800L, 21.1 ± 4.1 %, n = 15; p < 0.05; Figures 9B and 9C). However, by 30 min, the amount of internalized GluR1 was nearly identical between control neurons and EZ-disrupted neurons (GFP, 36.1 ± 1.7 %, n = 20; Dyn3-PRD, 33.5 ± 2.2 %, n = 19; Dyn3-P800L, 39.6 ± 4.3 %, n = 20; p > 0.05; Figures 9B and 9C). Uncoupling the EZ from the PSD had no effect on the uptake kinetics of transferrin (Figure 9D), as expected for a generic clathrin endocytic cargo whose receptor is more uniformly distributed over the dendritic plasma membrane. Thus, AMPA receptor endocytosis is selectively delayed in the absence of a PSD-associated EZ.

A second prediction of the model (Figure 9A) is that disruption of the EZ should impair synaptic recycling of AMPA receptors. To monitor AMPA receptor recycling, we performed antibody-based receptor recycling assays (Ehlers, 2000; Scott et al., 2004) (See Experimental Procedures and Supplemental Methods for details). Taking advantage of the 10–15% of glutamatergic synapses that lack an EZ, we compared the levels of recycled HA-GluR1 at EZ-positive and EZ-negative synapses. In contrast to the robust accumulation of recycled GluR1 at EZ-positive synapses, synapses lacking an EZ failed to accumulate recycled GluR1 (Figure 9E, Supplementary Figure S10). Even on occasions where adjacent EZ-positive and EZ-negative synapses were observed, recycled HA-GluR1 receptors accumulated selectively at the EZ-positive synapses (Figure 9E). Quantitative analysis revealed a >60% reduction in recycled

HA-GluR1 AMPA receptors at synapses lacking a nearby EZ (Figure 9F). Moreover, forced uncoupling of the EZ from the PSD by expression of Dyn3-PRD or Dyn3-P800L led to a profound reduction in recycled HA-GluR1 at VGLUT-positive synapses (GFP, 1.00 ± 0.02, n = 16; Dyn3-PRD, 0.18 ± 0.01, n = 12; Dyn3-P800L, 0.13 ± 0.01, n = 14; $p < 0.001$ relative to control; Figure 9G). Similar results were obtained for HA-GluR2 recycling in Dyn3-PRD or Dyn3-P800L expressing cells (GFP, 1.00 ± 0.05, n = 9; Dyn3-PRD, 0.34 ± 0.02 %, n = 7; Dyn3-P800L, 0.24 ± 0.02%, n = 7; $p < 0.001$ relative to control; Figure 9G). Interestingly, the surface level of recycled AMPA receptors at the extrasynaptic membrane was unaffected by spatial disruption of the EZ (GFP, 1.00 ± 0.03; Dyn3-PRD, 0.93 ± 0.03; Dyn3-P800L, 0.93 ± 0.04 %; $p > 0.05$ Figure 9H). The lack of synaptic AMPA receptor recycling upon disruption of dynamin-3 was not simply due to an overall impairment of endocytic trafficking, as neither the uptake nor recycling of the transferrin was affected by expression of Dyn3-PRD or Dyn3-P800L (Figure 9D and Figure 9I). These findings demonstrate that reaccumulation of recycled AMPA receptors at synapses requires localized endocytosis near the postsynaptic membrane. Thus, the EZ adjacent to the PSD maintains synaptic AMPA receptors by establishing a local endocytic cycling system near the postsynaptic membrane.

Discussion

In the present study, we have demonstrated that endocytic sites adjacent to the PSD are positioned and stabilized by a Shank-Homer-Dynamin-3 protein complex. Disruption of this complex leads to the physical uncoupling of the endocytic machinery from the PSD. The proximity of the EZ in turn enables a local cycle of endocytosis and recycling that maintains synaptic AMPA receptors at postsynaptic sites. At spines lacking endocytic zones, AMPA receptors released from the PSD diffuse away from the synapse for endocytosis at more distant sites. In this case, the absence of local cycling prevents cargo recapture, leading to a loss of AMPA receptors from the synapse.

Positioning Endocytic Machinery Near the PSD

Endocytosis and endosomal recycling of AMPA receptors regulates excitatory synaptic transmission (Derkach et al., 2007). We have previously shown that endocytosis of postsynaptic cargo occurs at endocytic sites situated adjacent to the PSD, defining a novel clathrin endocytic zone (EZ) (Blanpied et al., 2002; Racz et al., 2004). Yet it has been unclear how the clathrin endocytic machinery becomes stably positioned. Here we have shown that this abutting spatial arrangement is mediated by a physical interaction between the postsynaptic adaptor protein Homer and the large GTPase dynamin-3. The Dyn3-Homer complex is well-suited to couple the endocytic apparatus to the PSD since Homer binds the core PSD scaffold Shank, while dynamin-3 oligomerizes with both itself and dynamin-2 and associates with actin-based endocytic adaptors (Gray et al., 2005). Shank localizes to the deepest cytoplasmic face of the PSD (Valtschanoff and Weinberg, 2001) and forms large sheets composed of helical fibers stacked side by side (Baron et al., 2006). On the other hand, dynamins can organize extended actin networks (Schafer, 2004; Kruchten and McNiven, 2006) and can also homo-or hetero-oligomerize to form large stacked ring structures (Okamoto et al., 1999; Praefcke and McMahon, 2004). Thus, extended oligomeric structures of Shank and dynamin, linked by multimerized Homer (Hayashi et al., 2006), could plausibly bridge the PSD and the EZ.

Our results further suggest that protein interactions organizing the postsynaptic membrane extend laterally along the spine membrane. Both Shank and Homer are concentrated in the PSD, a membrane subregion comprising only ~15% of the spine plasma membrane. Beyond the PSD, the lateral spine membrane remains largely *terra incognita*. We have shown that the Homer binding partner dynamin-3 localizes to the lateral spine membrane, with a distribution that spans the PSD and the EZ. Moreover, selective disruption of the Dyn3-Homer interaction

or knock-down of endogenous dynamin-3 leads to the physical loss of the EZ from lateral spine domains. Protein interactions emanating from Homer-Shank may be a general feature of membrane organization at the periphery or more distant ‘suburbs’ of the spine. Such an organization could conceivably contribute to the addition or removal of membrane proteins at the edge of the PSD.

Dynamin-Family GTPases in Postsynaptic Compartments

At synapses, the vast majority of work on dynamin has centered on dynamin-1 and its prominent role in synaptic vesicle endocytosis. Though previously considered functionally interchangeable, recent studies have found distinct roles for dynamin isoforms in presynaptic vesicle cycling and synaptic transmission (Ferguson et al., 2007). At the postsynaptic membrane, dynamin-dependent endocytosis regulates excitatory synaptic transmission (Luscher et al., 1999) and AMPA receptor internalization (Carroll et al., 1999), and dynamin isoforms have been localized to dendritic spines (Gray et al., 2003; Racz et al., 2004), suggesting postsynaptic functions that have been poorly understood. Here we have shown that an interaction between dynamin-3 and the postsynaptic adaptor Homer recruits the endocytic machinery to dendritic spines.

In contrast to the GTPase-dependent regulation of postsynaptic receptor endocytosis that involves dynamin-2 (Luscher et al., 1999; Chowdhury et al., 2006), the scaffolding function of dynamin-3 appears to be independent of its GTPase activity and its participation in endocytosis. In dendritic spines, the coordination of Dyn3-dependent positioning of the endocytic machinery with Dyn2/Dyn3-mediated endocytosis is likely accomplished by the ability of dynamins to oligomerize (Okamoto et al., 1999). Here we have found that an oligomerization-deficient mutant of dynamin-3 uncouples clathrin puncta from sites adjacent to the PSDs. Together with the requirement for Homer binding, our results support a bifunctional model whereby oligomerization through its GTPase effector domain (GED) links dynamin-3 to the endocytic machinery while Homer-binding via its proline-rich domain couples dynamin-3 to the PSD. Intriguingly, at the *Drosophila* neuromuscular synapse, loss of the multivalent scaffold Eps15 causes a severe reduction in presynaptic dynamin and reduced synaptic transmission (Koh et al., 2007), suggesting that spatially restricted pools of dynamin must be locally concentrated for efficient endocytosis.

Previous studies have shown that dynamin-3 associates with the actin regulatory protein cortactin (Gray et al., 2005), which is recruited to clathrin coats during endocytosis (Kaksonen et al., 2006). Multiple splice variants of dynamin-3 are expressed in brain with differential abilities to regulate spines and actin remodeling (Gray et al., 2003; Gray et al., 2005). Interestingly, the positioning of EZ in spines is unaffected by actin polymerization or depolymerization (Blanpied et al., 2002). In addition, we have found that mutant dynamin-3 unable to bind cortactin has no effect on EZ localization, and forced uncoupling of the EZs does not change actin content or actin turnover in spines. Thus, the postsynaptic positioning of EZ by dynamin-3 is not an indirect effect of actin remodeling.

The Endocytic Zone Recaptures AMPA Receptors

A major determinant of synaptic strength at glutamatergic synapses is the number of postsynaptic AMPA receptors (Derkach et al., 2007). AMPA receptors are highly mobile, trafficking into and out of the dendritic membrane (Luscher et al., 1999; Ehlers, 2000) and diffusing into and out of the PSD (Tardin et al., 2003; Triller and Choquet, 2005; Ehlers et al., 2007). This raises the question as to how, once released from the postsynaptic scaffold, AMPA receptors are kept at synapses. Here we have shown that the tight coupling of the EZ with the PSD maintains AMPA receptors at the synapse, effectively sustaining excitatory synaptic transmission.

The EZ was originally envisioned to mediate facile endocytosis and therefore synaptic removal of receptors. We have found instead that uncoupling the EZ from the PSD leads to a marked loss of synaptic AMPA receptors. Thus, rather than being principally a mechanism for receptor removal, the EZ acts as a localized mechanism for receptor recapture. In this regard, it is interesting to note that internalization of extrasynaptic AMPA receptors precedes the removal of synaptic AMPA receptors (Ashby et al., 2004), and electrophysiological results support a role for a perisynaptic pool of AMPA receptors in rapid receptor exchange (Gardner et al., 2005).

Regulation of AMPA receptor endocytosis and recycling is a principal mechanism for activity-dependent synaptic plasticity, including long-term depression (LTD), long-term potentiation (LTP) (Derkach et al., 2007), and longer term homeostatic plasticity (Shepherd et al., 2006). Here we have shown that spatial uncoupling of the EZ from the PSD leads to reduced AMPA receptor-mediated synaptic transmission, a decrease in AMPAR/NMDAR ratios at excitatory synapses, and an increase in 'NMDAR-only' synapses. Such NMDAR-only or "postsynaptically silent" synapses are abundant early in development and can be converted to fully functioning AMPA receptor-containing synapses in response to LTP-inducing stimuli (Liao et al., 1995). Conversely, LTD-inducing stimuli promote the removal of synaptic AMPA receptors (Derkach et al., 2007). In principle, activity-dependent recruitment or stabilization of the endocytic machinery could tune the abundance of AMPA receptors by favoring or disfavoring synaptic recapture.

In presynaptic nerve terminals, the assembly and disassembly of endocytic proteins including dynamin are regulated by activity-dependent dephoshorylation and phosphorylation, respectively (Marks and McMahon, 1998; Slepnev et al., 1998). Interestingly, the very same kinase and phosphatase cascades are known to mediate postsynaptic plasticity and AMPA receptor trafficking (Derkach et al., 2007). Furthermore, although EZs are stably present in mature spines (Blanpied et al., 2002), recycling endosomes are increased in spines after LTP (Park et al., 2006), and key endocytic regulatory proteins respond to synaptic activity and intracellular signaling (Brown et al., 2005). Moreover, recent studies have shown that the activity-regulated gene products Arc/Arg3.1 and CPG2 exert their effects on synaptic function by regulating postsynaptic endocytosis (Cottrell et al., 2004; Chowdhury et al., 2006). Here we have shown that another activity-regulated gene product, the truncated Homer isoform Homer1a, disrupts the binding of dynamin-3 to Homer/Shank and thereby uncouples the spine EZ from the PSD, thus altering the spatial location of AMPA receptor cycling. Thus, diverse signaling pathways for activity-dependent postsynaptic plasticity converge on the spine endocytic machinery.

Establishing Spine-Specific Endocytic Cycling

Although postsynaptic membrane trafficking has emerged as a central mechanism for synapse development and modification, the cellular machinery for highly compartmentalized trafficking in dendritic spines is only now beginning to be revealed. Here we have shown that a physical link between the PSD and the spine endocytic machinery ensures localized endocytic trafficking. One consequence of such localized trafficking would be to 'focus' or restrict the membrane domain over which endocytic recycling can occur, allowing for both local and dynamic regulation of membrane composition on a spine-by-spine basis. First, endocytic zones near the PSD may provide efficient and fast internalization of nearby synaptic components, offering rapid regulation of factors displayed on the spine surface. Second, endocytic zones may help maintain the molecular composition of a given spine by preventing diffusion of membrane components to neighboring synapses. The presence of a continuously cycling EZ adjacent to the PSD, along with the restricted diffusion of membrane proteins out of the spine head, could sequester the components of a given synapse, explaining how individual spines

can maintain a unique and enduring identity. Such a mechanism may provide a general paradigm for localized regulation of cellular membrane composition on a micron scale.

Experimental Procedures

DNA constructs, cell culture, antibodies, immunocytochemistry, trafficking assays, and immunoprecipitation methods are included in the Supplemental Material.

Image Acquisition, Analysis and Quantification

For live cell imaging, confocal images were obtained using a Yokogawa spinning disk confocal (Solamere Technology Group). For fixed samples, images were acquired with a Leica TCS SP2 laser scanning confocal microscope. Images were analyzed using Metamorph (Universal Imaging Corporation). Detailed descriptions are available in the Supplemental Methods.

Electrophysiology

Whole-cell voltage clamp recordings were performed on DIV 17–24 hippocampal neurons cultured at high density on poly-lysine coated glass coverslips. See Supplemental Material for details.

Electron Microscopy

Immunogold labeling of adult rat CA1 hippocampus was performed with anti-Dyn3 antibody as described (Racz et al., 2004). Further methods are provided in the Supplemental Material.

RNA interference

Two separate DNA oligonucleotides specific to the rat dynamin-3 gene, a loop region (TTGATATCCG), and the antisense dynamin-3 sequence were annealed to their antisense counterparts and ligated into the pRNAT-H1.3-Hygro plasmid (Genscript). These shRNA constructs were transfected in cultured hippocampal neurons for 6 days *in vitro* using Lipofectamine 2000 (Invitrogen). The target shRNA sequences are listed in the Supplemental Methods.

Statistical Analysis

Unless otherwise stated, error bars represent the standard error of the mean and statistical comparisons were Student’s t tests.

Supplementary Material

Refer to Web version on PubMed Central for supplementary material.

Acknowledgments

We thank Marguerita Klein, Irina Lebedeva, and Haiwei Zhang for excellent technical assistance. We thank Ben Arenkiel, Daniel Choquet, Kathryn Condon, Ian Davison, Juliet Hernandez, Matt Kennedy, Yuanyue Mu, Mikyoung Park, Enrica Petrini, Cam Robinson and Jason Yi for critical review of the manuscript. This work was supported by grants from the NIH (to M.D.E. and R.J.W.). M.D.E. is an Investigator of the Howard Hughes Medical Institute.

References

Ashby MC, De La Rue SA, Ralph GS, Uney J, Collingridge GL, Henley JM. Removal of AMPA receptors (AMPARs) from synapses is preceded by transient endocytosis of extrasynaptic AMPARs. J Neurosci 2004;24:5172–5176. [PubMed: 15175386]

Ashby MC, Maier SR, Nishimune A, Henley JM. Lateral diffusion drives constitutive exchange of AMPA receptors at dendritic spines and is regulated by spine morphology. J Neurosci 2006;26:7046–7055. [PubMed: 16807334]

Baron MK, Boeckers TM, Vaida B, Faham S, Gingery M, Sawaya MR, Salyer D, Gundelfinger ED, Bowie JU. An architectural framework that may lie at the core of the postsynaptic density. Science 2006;311:531–535. [PubMed: 16439662]

Blanpied TA, Scott DB, Ehlers MD. Dynamics and regulation of clathrin coats at specialized endocytic zones of dendrites and spines. Neuron 2002;36:435–449. [PubMed: 12408846]

Brown TC, Tran IC, Backos DS, Esteban JA. NMDA receptor-dependent activation of the small GTPase Rab5 drives the removal of synaptic AMPA receptors during hippocampal LTD. Neuron 2005;45:81–94. [PubMed: 15629704]

Cao H, Garcia F, McNiven MA. Differential distribution of dynamin isoforms in mammalian cells. Mol Biol Cell 1998;9:2595–2609. [PubMed: 9725914]

Carroll RC, Beattie EC, Xia H, Luscher C, Altschuler Y, Nicoll RA, Malenka RC, von Zastrow M. Dynamin-dependent endocytosis of ionotropic glutamate receptors. Proc Natl Acad Sci U S A 1999;96:14112–14117. [PubMed: 10570207]

Chowdhury S, Shepherd JD, Okuno H, Lyford G, Petralia RS, Plath N, Kuhl D, Huganir RL, Worley PF. Arc/Arg3.1 interacts with the endocytic machinery to regulate AMPA receptor trafficking. Neuron 2006;52:445–459. [PubMed: 17088211]

Cook TA, Urrutia R, McNiven MA. Identification of dynamin 2, an isoform ubiquitously expressed in rat tissues. Proc Natl Acad Sci U S A 1994;91:644–648. [PubMed: 8290576]

Cottrell JR, Borok E, Horvath TL, Nedivi E. CPG2: a brain- and synapse-specific protein that regulates the endocytosis of glutamate receptors. Neuron 2004;44:677–690. [PubMed: 15541315]

Derkach VA, Oh MC, Guire ES, Soderling TR. Regulatory mechanisms of AMPA receptors in synaptic plasticity. Nat Rev Neurosci 2007;8:101–113. [PubMed: 17237803]

Ehlers MD. Reinsertion or degradation of AMPA receptors determined by activity-dependent endocytic sorting. Neuron 2000;28:511–525. [PubMed: 11144360]

Ehlers MD, Heine M, Groc L, Lee MC, Choquet D. Diffusional Trapping of GluR1 AMPA Receptors by Input-Specific Synaptic Activity. Neuron 2007;54:447–460. [PubMed: 17481397]

Ferguson SM, Brasnjo G, Hayashi M, Wolfel M, Collesi C, Giovedi S, Raimondi A, Gong LW, Ariel P, Paradise S, et al. A selective activity-dependent requirement for dynamin 1 in synaptic vesicle endocytosis. Science 2007;316:570–574. [PubMed: 17463283]

Gaidarov I, Santini F, Warren RA, Keen JH. Spatial control of coated-pit dynamics in living cells. Nat Cell Biol 1999;1:1–7. [PubMed: 10559856]

Gardner SM, Takamiya K, Xia J, Suh JG, Johnson R, Yu S, Huganir RL. Calcium-permeable AMPA receptor plasticity is mediated by subunit-specific interactions with PICK1 and NSF. Neuron 2005;45:903–915. [PubMed: 15797551]

Gerrow K, Romorini S, Nabi SM, Colicos MA, Sala C, El-Husseini A. A preformed complex of postsynaptic proteins is involved in excitatory synapse development. Neuron 2006;49:547–562. [PubMed: 16476664]

Gray NW, Fourgeaud L, Huang B, Chen J, Cao H, Oswald BJ, Hemar A, McNiven MA. Dynamin 3 is a component of the postsynapse, where it interacts with mGluR5 and Homer. Curr Biol 2003;13:510–515. [PubMed: 12646135]

Gray NW, Kruchten AE, Chen J, McNiven MA. A dynamin-3 spliced variant modulates the actin/cortactin-dependent morphogenesis of dendritic spines. J Cell Sci 2005;118:1279–1290. [PubMed: 15741233]

Hayashi MK, Ames HM, Hayashi Y. Tetrameric hub structure of postsynaptic scaffolding protein homer. J Neurosci 2006;26:8492–8501. [PubMed: 16914674]

Kaksonen M, Toret CP, Drubin DG. Harnessing actin dynamics for clathrin-mediated endocytosis. Nat Rev Mol Cell Biol 2006;7:404–414. [PubMed: 16723976]

Kennedy MJ, Ehlers MD. Organelles and trafficking machinery for postsynaptic plasticity. Annu Rev Neurosci 2006;29:325–362. [PubMed: 16776589]

Koh TW, Korolchuk VI, Wairkar YP, Jiao W, Evergren E, Pan H, Zhou Y, Venken KJ, Shupliakov O, Robinson IM, et al. Eps15 and Dap160 control synaptic vesicle membrane retrieval and synapse development. J Cell Biol 2007;178:309–322. [PubMed: 17620409]

Kruchten AE, McNiven MA. Dynamin as a mover and pincher during cell migration and invasion. J Cell Sci 2006;119:1683–1690. [PubMed: 16636070]

Liao D, Hessler NA, Malinow R. Activation of postsynaptically silent synapses during pairing-induced LTP in CA1 region of hippocampal slice. Nature 1995;375:400–404. [PubMed: 7760933]

Luscher C, Xia H, Beattie EC, Carroll RC, von Zastrow M, Malenka RC, Nicoll RA. Role of AMPA receptor cycling in synaptic transmission and plasticity. Neuron 1999;24:649–658. [PubMed: 10595516]

Marco E, Wedlich-Soldner R, Li R, Altschuler SJ, Wu LF. Endocytosis optimizes the dynamic localization of membrane proteins that regulate cortical polarity. Cell 2007;129:411–422. [PubMed: 17448998]

Marks B, McMahon HT. Calcium triggers calcineurin-dependent synaptic vesicle recycling in mammalian nerve terminals. Curr Biol 1998;8:740–749. [PubMed: 9651678]

Naisbitt S, Kim E, Tu JC, Xiao B, Sala C, Valtschanoff J, Weinberg RJ, Worley PF, Sheng M. Shank, a novel family of postsynaptic density proteins that binds to the NMDA receptor/PSD-95/GKAP complex and cortactin. Neuron 1999;23:569–582. [PubMed: 10433268]

Nakata T, Iwamoto A, Noda Y, Takemura R, Yoshikura H, Hirokawa N. Predominant and developmentally regulated expression of dynamin in neurons. Neuron 1991;7:461–469. [PubMed: 1832879]

Okamoto PM, Gamby C, Wells D, Fallon J, Vallee RB. Dynamin isoform-specific interaction with the shank/ProSAP scaffolding proteins of the postsynaptic density and actin cytoskeleton. J Biol Chem 2001;276:48458–48465. [PubMed: 11583995]

Okamoto PM, Tripet B, Litowski J, Hodges RS, Vallee RB. Multiple distinct coiled-coils are involved in dynamin self-assembly. J Biol Chem 1999;274:10277–10286. [PubMed: 10187814]

Park M, Penick EC, Edwards JG, Kauer JA, Ehlers MD. Recycling endosomes supply AMPA receptors for LTP. Science 2004;305:1972–1975. [PubMed: 15448273]

Park M, Salgado JM, Ostroff L, Helton TD, Robinson CG, Harris KM, Ehlers MD. Plasticity-induced growth of dendritic spines by exocytic trafficking from recycling endosomes. Neuron 2006;52:817–830. [PubMed: 17145503]

Praefcke GJ, McMahon HT. The dynamin superfamily: universal membrane tubulation and fission molecules? Nat Rev Mol Cell Biol 2004;5:133–147. [PubMed: 15040446]

Racz B, Blanpied TA, Ehlers MD, Weinberg RJ. Lateral organization of endocytic machinery in dendritic spines. Nat Neurosci 2004;7:917–918. [PubMed: 15322548]

Sala C, Futai K, Yamamoto K, Worley PF, Hayashi Y, Sheng M. Inhibition of dendritic spine morphogenesis and synaptic transmission by activity-inducible protein Homer1a. J Neurosci 2003;23:6327–6337. [PubMed: 12867517]

Sala C, Piech V, Wilson NR, Passafaro M, Liu G, Sheng M. Regulation of dendritic spine morphology and synaptic function by Shank and Homer. Neuron 2001;31:115–130. [PubMed: 11498055]

Schafer DA. Regulating actin dynamics at membranes: a focus on dynamin. Traffic 2004;5:463–469. [PubMed: 15180823]

Scott DB, Michailidis I, Mu Y, Logothetis D, Ehlers MD. Endocytosis and degradative sorting of NMDA receptors by conserved membrane-proximal signals. J Neurosci 2004;24:7096–7109. [PubMed: 15306643]

Sheng M, Hoogenraad CC. The Postsynaptic Architecture of Excitatory Synapses: A More Quantitative View. Annu Rev Biochem 2007;76:823–847. [PubMed: 17243894]

Shepherd JD, Rumbaugh G, Wu J, Chowdhury S, Plath N, Kuhl D, Huganir RL, Worley PF. Arc/Arg3.1 Mediates Homeostatic Synaptic Scaling of AMPA Receptors. Neuron 2006;52:475–484. [PubMed: 17088213]

Slepnev VI, Ochoa GC, Butler MH, Grabs D, De Camilli P. Role of phosphorylation in regulation of the assembly of endocytic coat complexes. Science 1998;281:821–824. [PubMed: 9694653]

Tardin C, Cognet L, Bats C, Lounis B, Choquet D. Direct imaging of lateral movements of AMPA receptors inside synapses. Embo J 2003;22:4656–4665. [PubMed: 12970178]

Triller A, Choquet D. Surface trafficking of receptors between synaptic and extrasynaptic membranes: and yet they do move! Trends Neurosci 2005;28:133–139. [PubMed: 15749166]

Tu JC, Xiao B, Naisbitt S, Yuan JP, Petralia RS, Brakeman P, Doan A, Aakalu VK, Lanahan AA, Sheng M, Worley PF. Coupling of mGluR/Homer and PSD-95 complexes by the Shank family of postsynaptic density proteins. Neuron 1999;23:583–592. [PubMed: 10433269]

Tu JC, Xiao B, Yuan JP, Lanahan AA, Leoffert K, Li M, Linden DJ, Worley PF. Homer binds a novel proline-rich motif and links group 1 metabotropic glutamate receptors with IP3 receptors. Neuron 1998;21:717–726. [PubMed: 9808459]

Valtschanoff JG, Weinberg RJ. Laminar organization of the NMDA receptor complex within the postsynaptic density. J Neurosci 2001;21:1211–1217. [PubMed: 11160391]

Washbourne P, Liu XB, Jones EG, McAllister AK. Cycling of NMDA receptors during trafficking in neurons before synapse formation. J Neurosci 2004;24:8253–8264. [PubMed: 15385609]

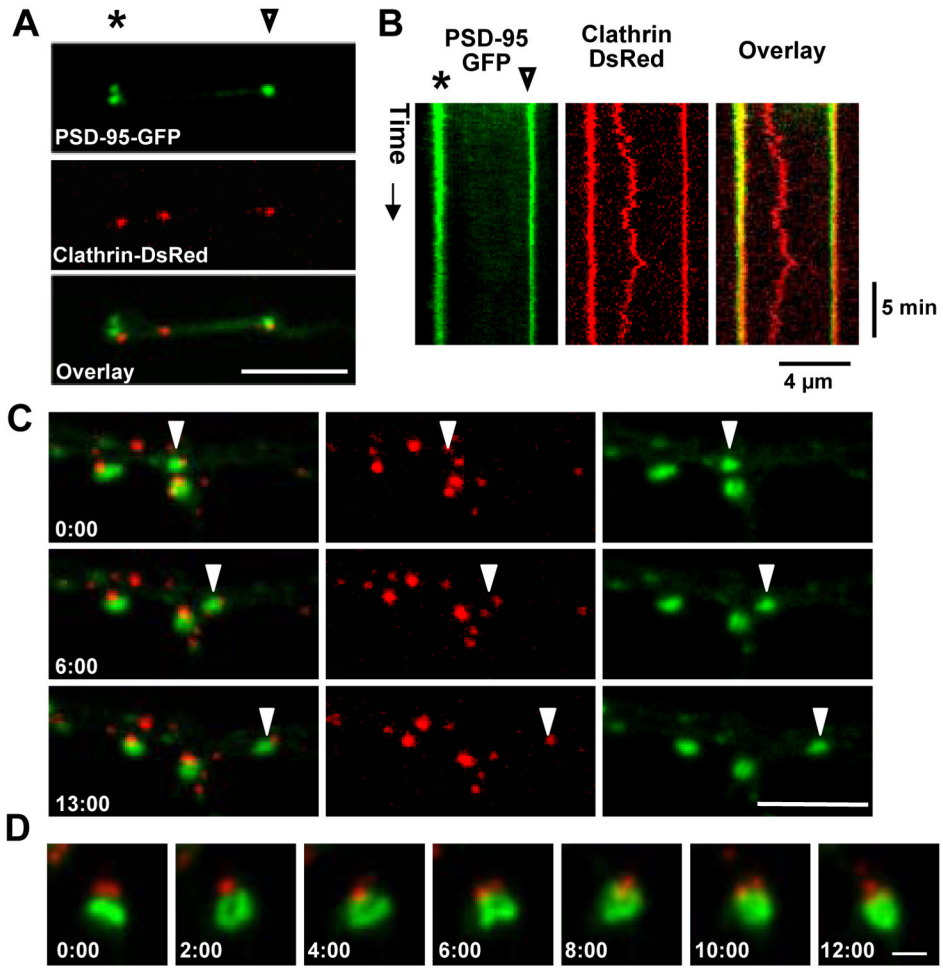

Figure 1. The Endocytic Zone is Stably Positioned Near the PSD

(**A**) Dendritic branch of a hippocampal neuron (17 DIV) co-expressing PSD-95-GFP and clathrin-DsRed. Scale bar, 4 μm. The asterisk and arrowhead mark points along the dendrite used for the kymograph analysis in (B).

(**B**) Kymograph analysis of fluorescence intensity along the dendritic branch (horizontal) over time (vertical) during a time lapse with images acquired every 14 sec. The asterisk and arrowhead mark points along the dendrite corresponding to positions in (A). See Supplementary Movie S1.

(**C**) The occasional mobile cluster of PSD-95 (arrowhead, green) continues to have an associated clathrin punctum (red). The structure moved at an average rate of 0.20 μm/min. Time in min:sec is indicated. Scale bar, 5 μm. See Supplementary Movie S2.

(**D**) Clathrin (red) remains near the PSD (green) even as it undergoes changes in size and morphology. Time in min:sec is indicated. Scale bar, 1 μm. See Supplementary Movie S3.

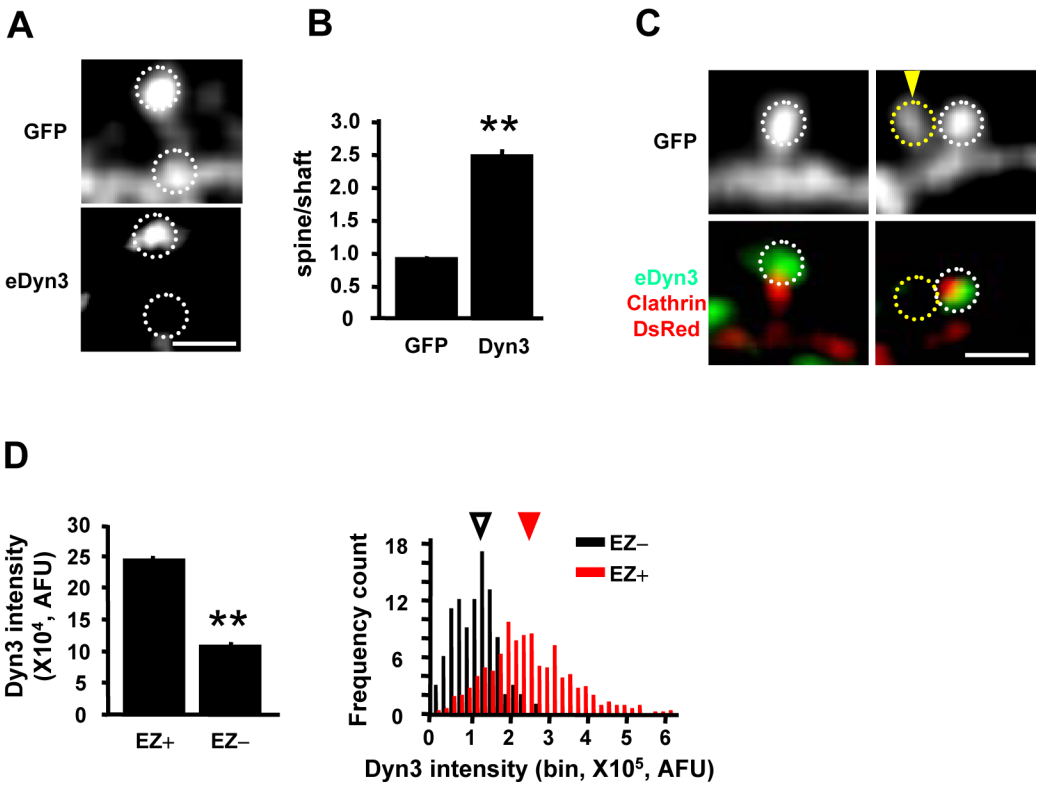

Figure 2. Dynamin-3 Concentrates in Dendritic Spines and Correlates with the Presence of an Endocytic Zone

(**A**) Confocal image of endogenous dynamin-3 (eDyn3) staining in a hippocampal neuron (DIV 34) expressing GFP. White dashed circles indicate regions selected for spine and shaft intensity measurement. Scale bar, 2 μm.

(**B**) Quantification of spine enrichment. Data represent means ± SEM of spine/shaft fluorescence intensity ratios. n = 8 neurons, 270 spines respectively, ** $p < 0.001$ relative to GFP, t-test.

(**C**) Confocal images of endogenous dynamin-3 (eDyn3) staining in hippocampal neurons expressing GFP and clathrin-DsRed. Spines lacking dynamin-3 also lacked clathrin (yellow dashed circle, arrowhead). Scale bar, 2 μm.

(**D**) Quantification of dynamin-3 (Dyn3) in spines that contain (EZ+) or lack (EZ−) an endocytic zone. Integrated Dyn3 intensity in the dashed circles was measured. Left, means ± SEM of dynamin-3 fluorescence intensity. EZ+, 557 spines, EZ−, 98 spines; n = 9 neurons; ** $p < 0.001$ relative to EZ+ spines, t-test. Right, histogram analysis of dynamin-3 fluorescence intensity in EZ− and EZ+ spines. Arrowheads indicate median values. AFU, arbitrary fluorescence units.

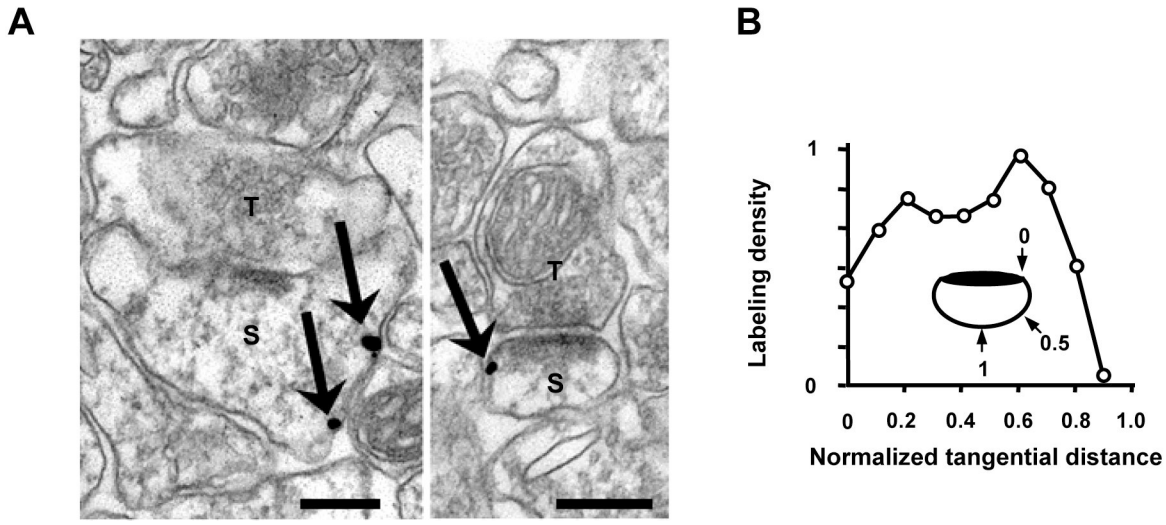

Figure 3. Dynamin-3 Localizes to Spine Membrane Domains Lateral to the PSD

(**A**) Electron micrographs from adult rat CA1 hippocampus indicating immunogold labeling for dynamin-3 (arrows). Dynamin-3 localizes to lateral spine membranes domains. S, spine; T, presynaptic terminal. Scale bars, 200 nm.

(**B**) Quantitative analysis of dynamin-3 immunogold particle density associated with the spine membrane plotted against tangential distance normalized by spine size (see inset). See Experimental Procedures for details.

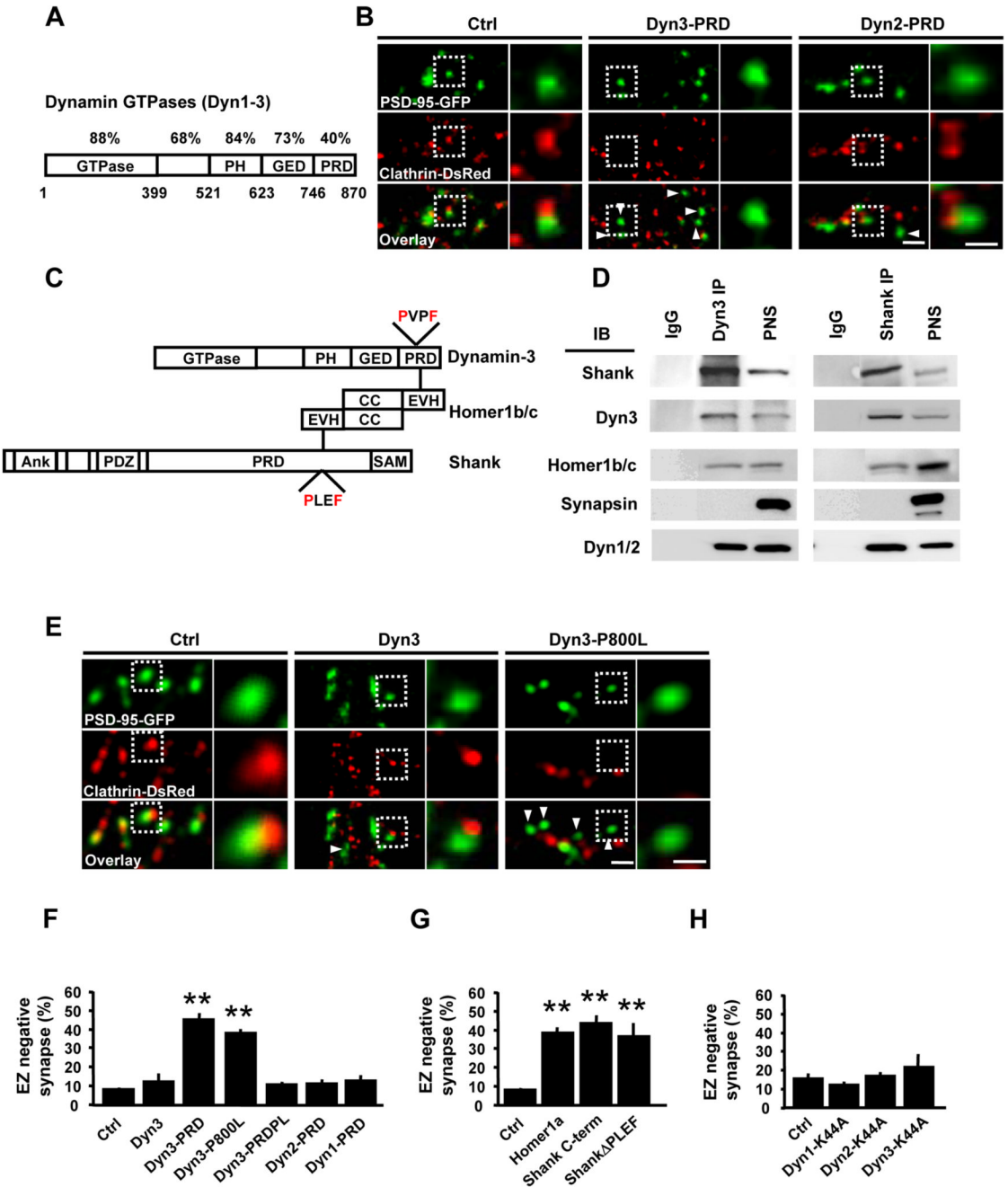

Figure 4. A Dyn3-Homer-Shank Protein Complex Couples the EZ and the PSD

(**A**) Schematic diagram of dynamin family GTPases illustrating their domain organization. The percent amino acid conservation between dynamins 1–3 for each separate protein domain is indicated. PH, pleckstrin homology domain; GED, GTPase effector domain; PRD, proline-rich domain. Bottom numbers are amino acid positions corresponding to dynamin-3.

(**B**) Expression of Dyn3-PRD uncouples the EZ from the PSD. Images are of hippocampal neurons expressing PSD-95-GFP and clathrin-DsRed together with the indicated Flag-tagged dynamin constructs. Right panels correspond to regions in the dashed white boxes. Scale bars, 2 μm and 1 μm.

(**C**) Schematic representation of protein interactions linking dynamin-3, Homer1b/c, and Shank. PH, pleckstrin homology domain; GED, GTPase effector domain; PRD, proline-rich domain; EVH1, Ena/Vasp homology domain 1; PXXF, consensus EVH1-binding motifs; Ank, ankyrin repeats; PDZ, PSD-95/discs-large/ZO-1 homology domain; SAM, sterile alpha motif.
(**D**) Dynamin-3 forms a complex with Homer and Shank in rat brain. Immunoprecipitations (IP) were performed with antibodies against either dynamin-3 (Dyn3) or Shank or with control IgG and precipitated proteins subjected to immunoblot analysis (IB) for the indicated proteins. PNS, postnuclear supernatant.
(**E**) The Homer binding domain of dynamin-3 is required for PSD-EZ coupling. Images correspond to dendritic segments of hippocampal neurons expressing PSD-95-GFP (green) and clathrin-DsRed (red) along with either wildtype (Dyn3) or Homer-binding deficient mutant (Dyn3-P800L) dynamin-3 constructs. Scale bars, 2 μm and 1 μm. Arrowheads indicate EZ-negative PSD-95 puncta.
(**F**) Quantitative analysis of PSD-associated endocytic machinery. Data represent means ± SEM of the fraction of synapses lacking a clathrin-DsRed punctum within 0.7 μm (EZ-negative synapses) on hippocampal neurons expressing the indicated constructs. n = 134, 15, 20, 34, 27, 16, and 20 from left to right; ** $p < 0.001$ relative to control, t-test.
(**G**) Disruption of Homer and Shank interactions causes loss of the spine EZ. Data represent means ± SEM of the fraction of EZ-negative synapses on hippocampal neurons expressing the indicated constructs. n = 134, 37, 12, and 21 from left to right; ** $p < 0.001$ relative to control, t-test.
(**H**) GTPase-deficient mutant dynamins do not affect clathrin localization adjacent to the PSD. Data and analysis as in (F) and (G). n = 20, 15, 12, and 16, respectively; $p > 0.05$ relative to control, t-test.

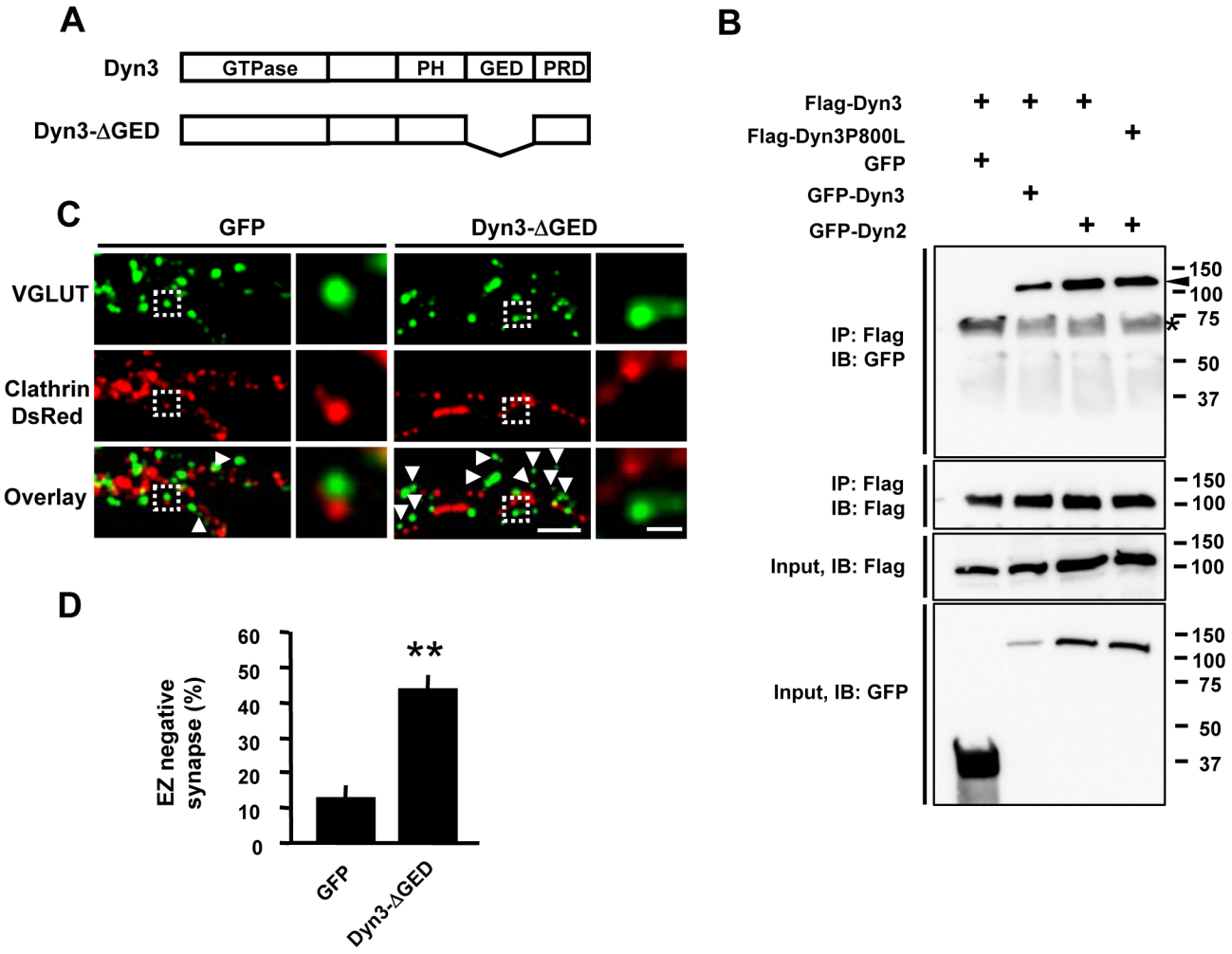

Figure 5. Oligomerization of Dynamin-3 is Required to Link the Endocytic Machinery to the PSD

(**A**) Schematic diagram of wild type and deletion mutant constructs of dynamin-3. PH, pleckstrin homology domain; GED, GTPase effector domain; PRD, proline-rich domain.

(**B**) Dynamin-3 forms both homo- and hetero-oligomers in HEK 293T cells. HEK 293T cells were co-transfected with Flag- and GFP-tagged dynamin-2 or dynamin-3. Immunoprecipitations (IP) were performed with an antibody against the Flag epitope and precipitated proteins subjected to immunoblot analysis (IB) for the indicated proteins. Inputs represent lysates used for IPs. Molecular mass in kilodaltons is shown at the right. The arrowhead indicates immunoprecipitated GFP-dynamin. The asterisk indicates a non-specific band.

(**C**) Expression of the oligomerization-deficient dynamin-3 mutant Dyn3-ΔGED uncouples the EZ from the PSD. Images are of hippocampal neurons expressing either Dyn3-ΔGED or GFP together with clathrin-DsRed. Cells were fixed and stained for the excitatory synapse marker VGLUT1. Right panels correspond to regions in the dashed white boxes. Scale bars, 5 μm and 1 μm. Arrowheads indicate EZ-negative VGLUT1 puncta.

(**D**) Quantification of EZ-negative synapses in neurons expressing Dyn3-ΔGED or GFP control. Data represent means ± SEM. n = 14, 8; ** $p < 0.001$ relative to GFP, t-test.

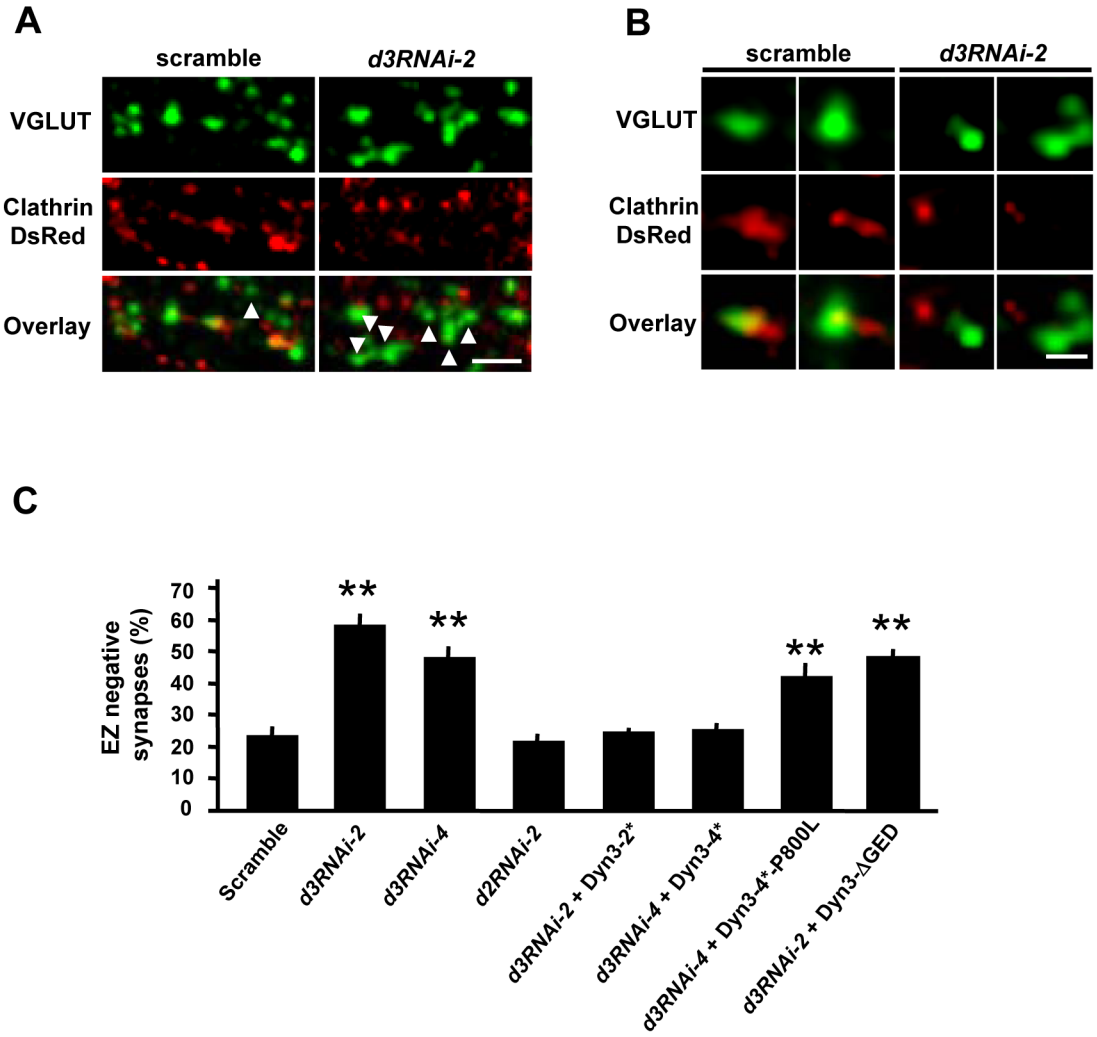

Figure 6. Endogenous Dynamin-3 is Required for Postsynaptic Positioning of the Endocytic Zone

(**A**) Dynamin-3 knock-down causes loss of the EZ. Hippocampal neurons expressing either dynamin-3 shRNA (*d3RNAi-2*) or a scrambled shRNA control (scramble) together with clathrin-DsRed were fixed and stained for VGLUT1. Scale bar, 5 μm.

(**B**) High magnification views of glutamatergic synapses (VGLUT1, green) and postsynaptic clathrin (clathrin-DsRed, red). Postsynaptic neurons expressed the indicated shRNA constructs. Scale bar, 1 μm.

(**C**) Quantification of endocytic zone (EZ) negative synapses in neurons expressing dynamin-3 shRNAs (*d3RNAi-2*, *d3RNAi-4*), dynamin-2 shRNA (*d2RNAi-2*) or a scrambled RNAi control. Co-expression of RNAi-resistant dynamin-3 cDNAs (Dyn3-2*, Dyn3–4*, Dyn3–4*-P800L, Dyn3-ΔGED) is indicated. Data are means ± SEM. n = 36, 41, 40, 13, 18, 25, 11 and 16, respectively; ** $p < 0.001$ relative to scrambled shRNA control, t-test.

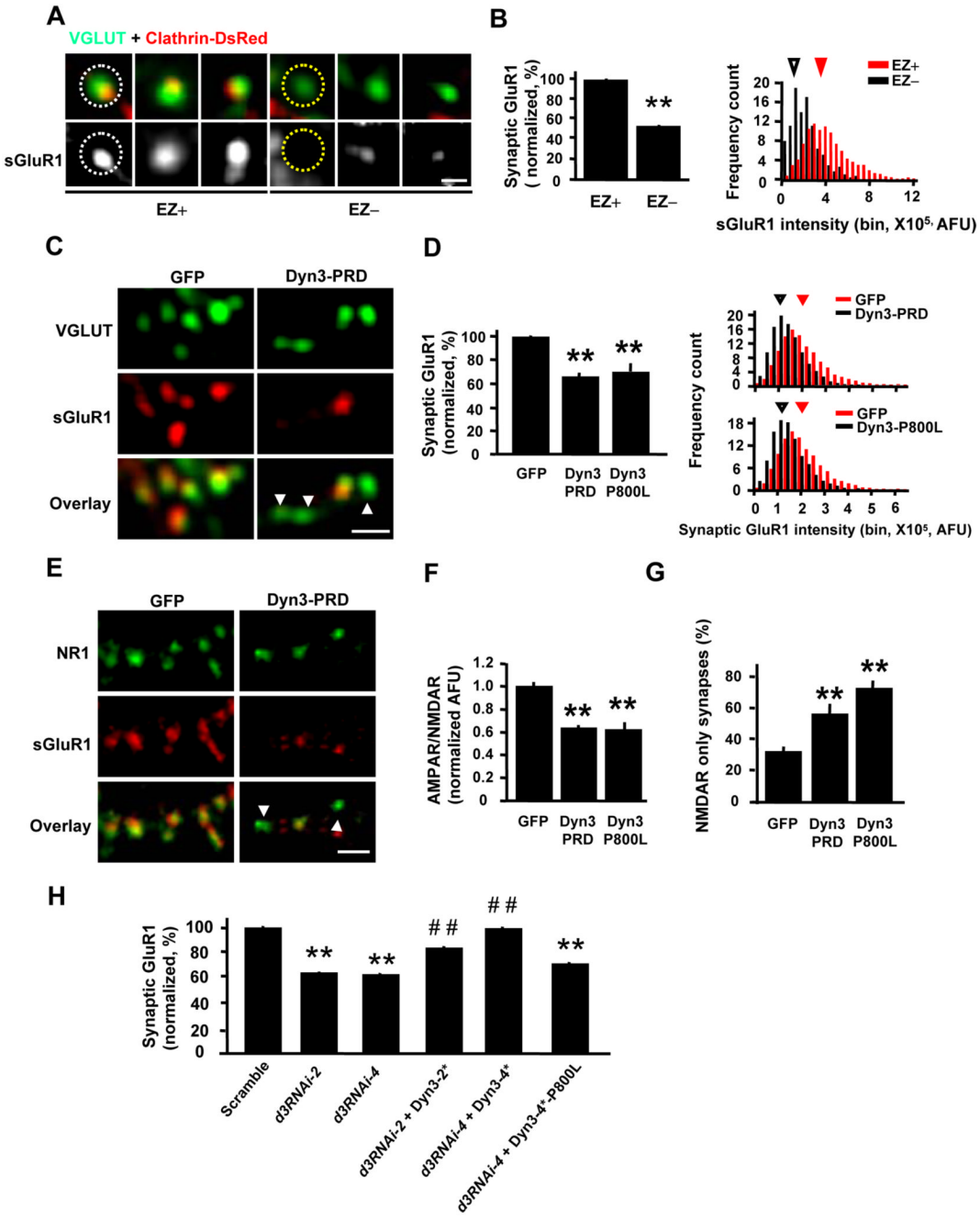

Figure 7. Uncoupling the EZ from the PSD Causes Loss of Synaptic AMPA Receptors

(**A**) AMPA receptors are more abundant in spines containing an EZ. Synaptic AMPA receptors on hippocampal neurons were visualized by surface GluR1 (sGluR1) staining. Spines containing (EZ+) or lacking (EZ−) an EZ were defined by the presence or absence of clathrin-DsRed. VGLUT1 was used to mark glutamatergic synapses. Scale bar, 1 μm. Dashed circles indicate regions selected for intensity measurement.

(**B**) Quantification of GluR1 in spines that contain (EZ+) or lack (EZ−) an EZ. Left, means ± SEM of surface GluR1 fluorescence intensity. n = 14 neurons, EZ+, 1635 synapses; EZ−, 319 synapses; ** $p < 0.001$ relative to EZ+ spines, t-test. Right, histogram analysis of surface GluR1 fluorescence intensity in EZ− and EZ+ spines. Arrowheads indicate median values.

(**C**) Disruption of the EZ decreases synaptic AMPA receptors. Endogenous surface GluR1 (sGluR1) and VGLUT1 were visualized by immunostaining of hippocampal neurons expressing either GFP or Dyn3-PRD. Arrowheads indicate synapses with undetectable levels of surface GluR1. Scale bar, 2 μm.

(**D**) Quantification of GluR1 at synapses expressing the indicated constructs. Left, means ± SEM of surface GluR1 fluorescence intensity. n = 20, 31, and 21, ** $p < 0.001$ relative to GFP, t-test. Right, histogram analysis of surface GluR1 fluorescence. Arrowheads indicate median values.

(**E**) Disruption of the EZ does not affect synaptic NMDA receptors. Endogenous surface GluR1 (sGluR1) and NR1 were visualized by immunostaining of hippocampal neurons (DIV 14–20) expressing either GFP or Dyn3-PRD. Arrowheads indicate synapses with little to no detectable GluR1, but which still contain NR1. Scale bar, 5 μm.

(**F**) Data represent means ± SEM of the normalized surface GluR1 (AMPAR) to NR1 (NMDAR) ratio at synapses on hippocampal neurons expressing the indicated constructs. n = 15, 16, and 11; ** $p < 0.001$, t-test.

(**G**) Quantification of NMDA receptor (NMDAR)-only synapses. ** $p < 0.001$ relative to GFP control, t-test. Error bars indicate SEM.

(**H**) Quantification of surface synaptic GluR1 on neurons expressing dynamin-3 shRNAs (*d3RNAi-2*, *d3RNAi-4*) or a scrambled RNAi control. Co-expression of RNAi-resistant dynamin-3 cDNAs (Dyn3-2*, Dyn3–4*, Dyn3–4*-P800L) is indicated. Data are means ± SEM. n values are 58, 36, 43, 19, 24, 16 and 19; ** $p < 0.001$ relative to scrambled RNAi control, ## $p < 0.001$ relative to corresponding RNAi construct; t-test.

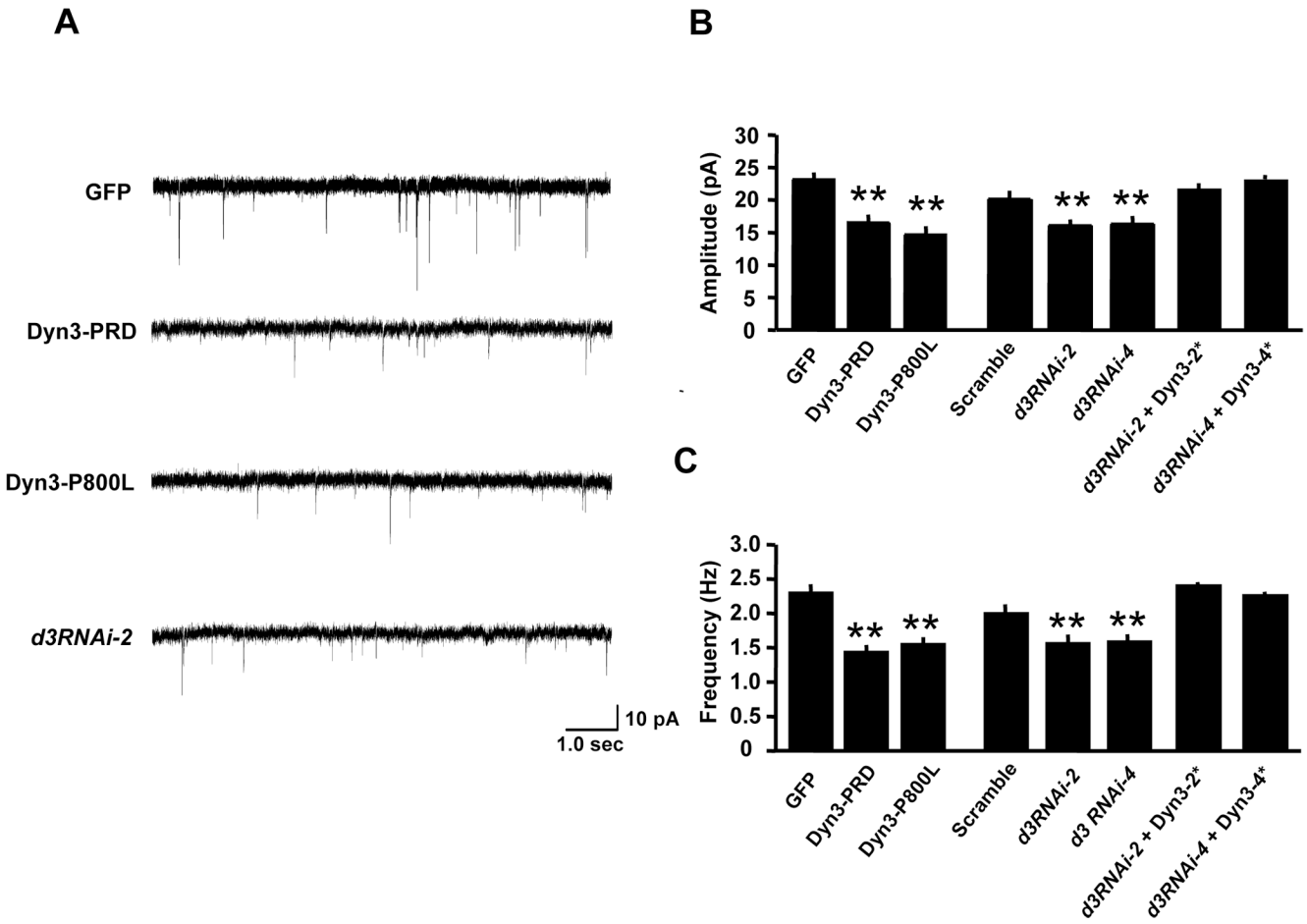

Figure 8. Disrupting the EZ Attenuates Excitatory Synaptic Transmission

(**A**) Representative traces showing AMPA receptor-mediated miniature excitatory postsynaptic currents (mEPSCs) recorded at DIV 17–24 from a control GFP-expressing hippocampal neuron (upper trace) and neurons expressing Dyn3-PRD, Dyn3-P800L, and *d3RNAi-2*.

(**B–C**) Quantitative analysis of mEPSC amplitudes (B) and frequencies (C). Data represent means ± SEM. n values are 20, 18, 20, 19, 16, 14, 15 and 13, respectively. ** $p < 0.001$ relative to control; t-test.

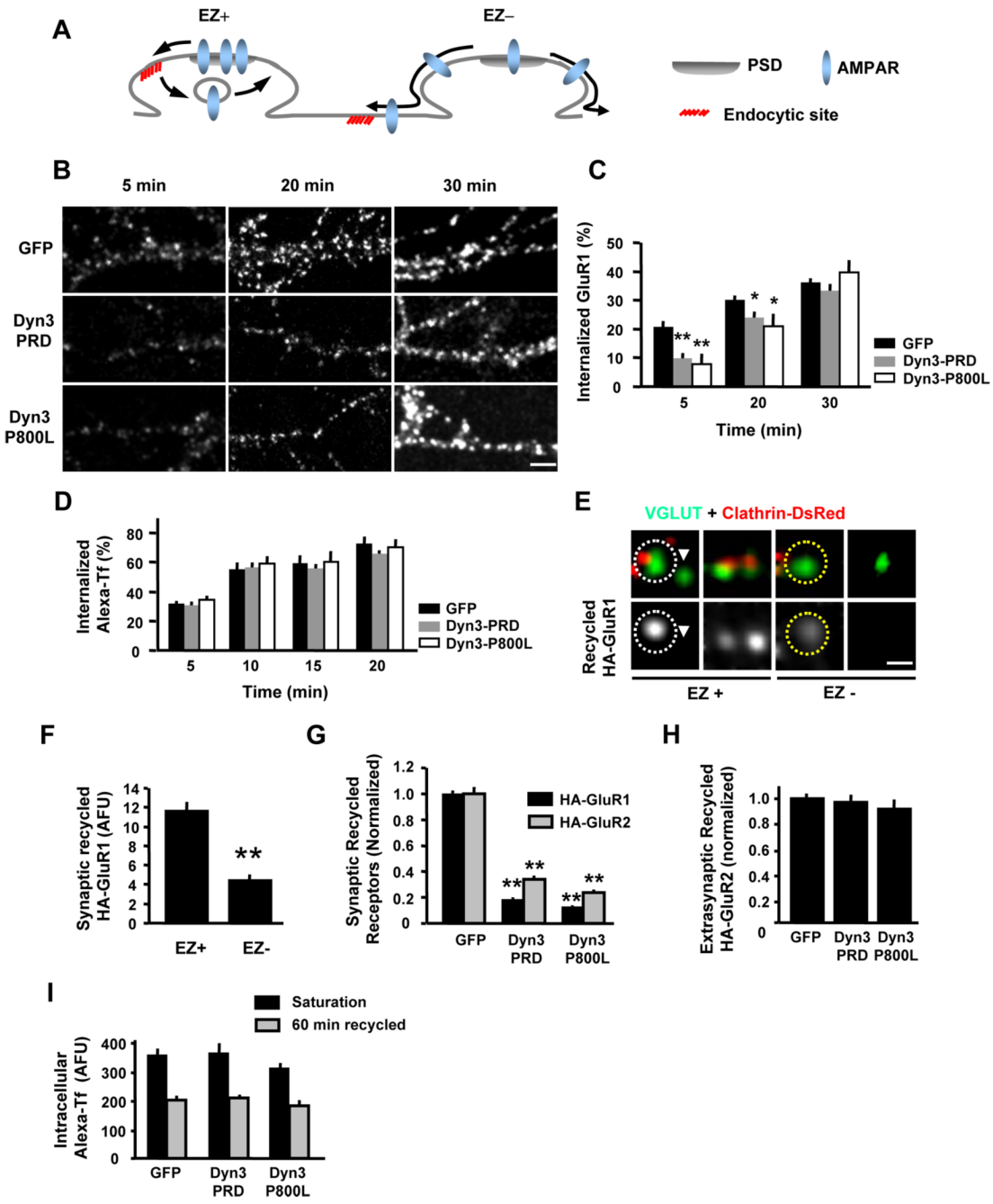

Figure 9. Uncoupling the EZ from the PSD Impairs Local Synaptic Recycling

(**A**) Proposed model for synaptic AMPA receptor endocytosis and recycling at synapses containing (EZ+) or lacking (EZ−) a PSD-associated EZ. The presence of an EZ ensures recapture of AMPA receptors (AMPARs) by localized recycling. Absent an EZ, AMPA receptors released from the PSD diffuse away from the synapse.

(**B**) Disruption of the dynamin-3/Homer complex slows AMPA receptor endocytosis. Antibody-based endocytosis assays were performed on hippocampal neurons expressing either EGFP, Dyn3-PRD or Dyn3-P800L (14–20 DIV) and internalized GluR1 was visualized at the indicated time points. See Experimental Procedures for details. Scale bar, 5 μm.

(**C**) Quantification of the results in (B). Data represent means ± SEM of internalized GluR1 at various times after incubation at 37°C normalized to total surface-labeled receptor at time zero. GFP, n = 17, 20 and 20; Dyn3-PRD, n = 20, 20 and 19; Dyn3-P800L, n = 20, 15 and 20; * $p < 0.05$, ** $p < 0.001$, comparisons between cells expressing EGFP and cells expressing Dyn3 constructs, unpaired t-test.
(**D**) Transferrin (Tf) endocytosis is unaltered in neurons expressing Dyn3-PRD or Dyn3-P800L. Data represent means ± SEM of internalized Alexa-Tf at various times after incubation at 37°C normalized to total surface-labeled receptor at time zero.
(**E**) Reduced recycling of GluR1 at EZ-negative synapses. Hippocampal neurons (14–20 DIV) co-expressing HA-GluR1 and clathrin-DsRed were incubated live with an anti-HA antibody at 10°C for 20 min followed by incubation at 37°C for 30 min to allow endocytosis. Remaining surface HA-GluR1 was blocked with unlabeled mouse secondary antibody. Neurons were then incubated for 1 hr at 37°C to allow recycling of internalized receptors. After fixation, recycled AMPA receptors on the surface were detected with Alexa568-conjugated secondary antibody. Glutamatergic synapses were labeled following permeabilization by staining for VGLUT1. Synapses lacking postsynaptic clathrin (EZ−) had less recycled GluR1, even when immediately next to an EZ-positive (EZ+) synapses (arrowhead). See Experimental Procedures for details. Scale bar, 1 μm.
(**F**) Data represent means ± SEM of recycled HA-GluR1 at EZ-positive (EZ+) and EZ-negative (EZ−) synapses. EZ+, 156 synapses; EZ−, 124 synapses; ** $p < 0.001$, unpaired t-test.
(**G**) Disrupting dynamin-3 binding to Homer prevents AMPA receptor synaptic recycling. Live antibody feeding and receptor recycling assays were performed as in (E) on hippocampal neurons expressing GFP, Dyn3-PRD, or Dyn3-P800L as indicated. Data represent means ± SEM of recycled HA-GluR1 or HA-GluR2 at VGLUT-positive synapses. n = 16, 12 and 14 for HA-GluR1; n = 9, 7 and 7 for HA-GluR2; ** $p < 0.001$, t-test.
(**H**) Extrasynaptic GluR2 recycling is unaltered in neurons expressing dynamin-3 mutants. Data represent means ± SEM of recycled HA-GluR2 fluorescence at extrasynaptic dendritic regions. n = 9, 7, 7; $p > 0.05$ relative to control, t-test.
(**I**) Neither uptake nor recycling of Tf is affected by disrupting the dynamin-3/Homer interaction. Hippocampal neurons expressing GFP, Dyn3-PRD, or Dyn3-P800L were incubated with Alexa-Tf for 60 min to allow saturating uptake (Saturation) followed by wash out and incubation with excess unlabeled transferrin (60 min recycled). Loss of internalized Tf fluorescence reflects recycling. See Experimental Procedures for details.